iScience

CellPress
OPEN ACCESS

Article

YTHDF3 modulates the Cbln1 level by recruiting BTG2 and is implicated in the impaired cognition of prenatal hypoxia offspring

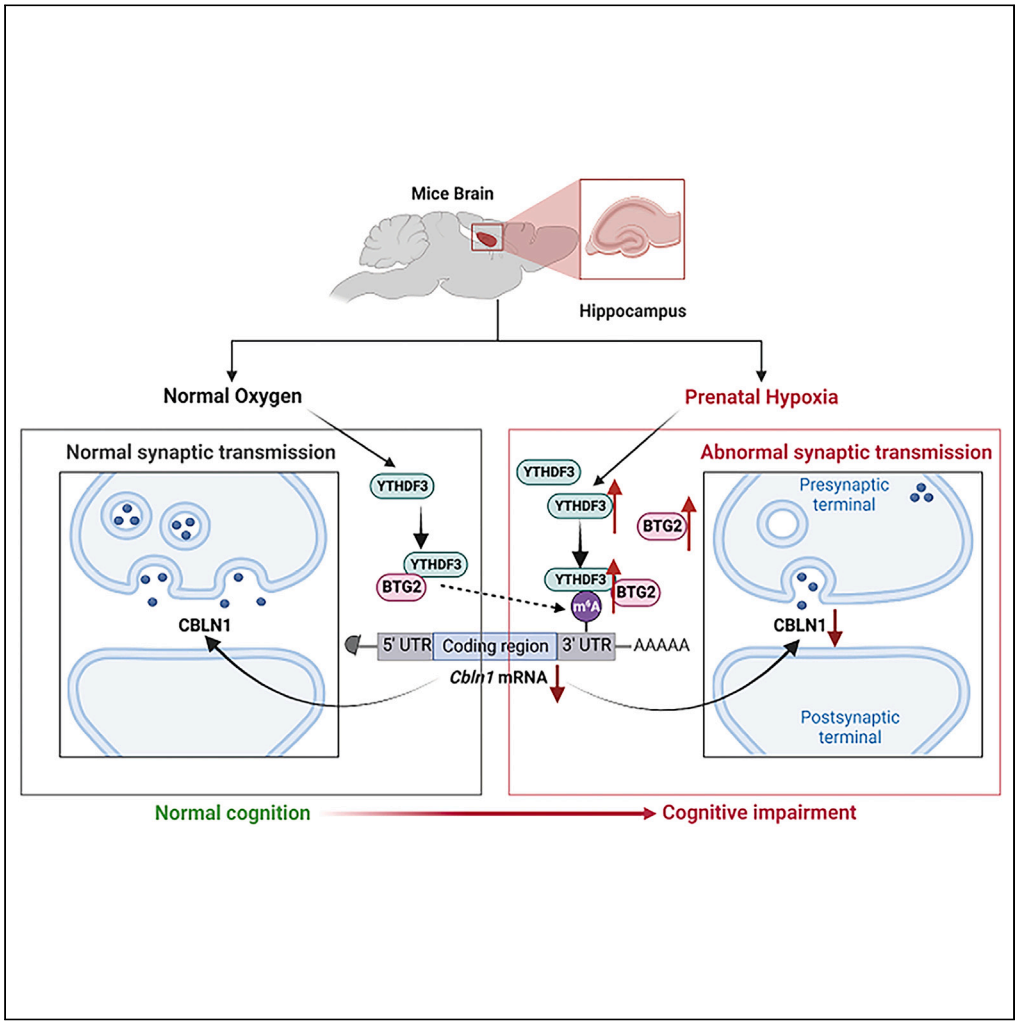

Likui Lu, Yajun Shi, Bin Wei, ..., Yan Zhao, Dongyi Yu, Miao Sun

miaosunsuda@163.com

Highlights

Prenatal hypoxia (PH) impaired spatial learning and memory in adult offspring

Cbln1 dysfunction may contribute to the cognition impairment of PH offspring

YTHDF3 destabilizes *Cbln1* mRNA in an m^{6}A-dependent manner by recruiting BTG2

Lu et al., iScience *27*, 108703
January 19, 2024
https://doi.org/10.1016/j.isci.2023.108703

iScience

CellPress
OPEN ACCESS

Article

YTHDF3 modulates the Cbln1 level by recruiting BTG2 and is implicated in the impaired cognition of prenatal hypoxia offspring

Likui Lu,[1,2,6] Yajun Shi,[1,6] Bin Wei,[1] Weisheng Li,[3] Xi Yu,[1] Yan Zhao,[1] Dongyi Yu,[4] and Miao Sun[1,5,7,*]

SUMMARY

The "Fetal Origins of Adult Disease (FOAD)" hypothesis holds that adverse factors during pregnancy can increase the risk of chronic diseases in offspring. Here, we investigated the effects of prenatal hypoxia (PH) on brain structure and function in adult offspring and explored the role of the N6-methyladenosine (m^6A) pathway. The results suggest that abnormal cognition in PH offspring may be related to the dysregulation of the m^6A pathway, specifically increased levels of YTHDF3 in the hippocampus. YTHDF3 interacts with BTG2 and is involved in the decay of *Cbln1* mRNA, leading to the down-regulation of *Cbln1* expression. Deficiency of Cbln1 may contribute to abnormal synaptic function, which in turn causes cognitive impairment in PH offspring. This study provides a scientific clues for understanding the mechanisms of impaired cognition in PH offspring and provides a theoretical basis for the treatment of cognitive impairment in offspring exposed to PH.

INTRODUCTION

The embryonic phase is a critical and sensitive period in one's development, during which both genetic and environmental factors have a significant impact on fetal growth and development. Changes in the maternal environment may alter the intrauterine condition, potentially causing subtle insults to the fetus and promoting increased lifetime disease risk and disease acceleration during childhood and later in life. David Barker first proposed the "Fetal Origins of Adult Disease (FOAD)" hypothesis in the 1990 s based on large numbers of epidemiological investigations. For example, Barker et al. found that low birth weight (a surrogate marker of poor fetal growth and nutrition) is associated with an increased risk of cardiovascular disease in adulthood.[1] The FOAD hypothesis holds that events during early development have a profound impact on one's risk for the development of future adult disease.[2] The formulation of the FOAD hypothesis has drawn considerable attention to the adverse intrauterine environment and its impact on adult disease. At the present, extensive research carried out by a large number of researchers lends credence to the FOAD concept. For example, many epidemiological studies on humans have demonstrated a link between adverse prenatal and neonatal environments and the occurrence of various health issues in offspring during their adult years,[3–7] including abnormalities in neurological function.[8,9] However, epidemiological studies may be confounded by extraneous factors, so more evidence is needed to confirm the reliability of the FOAD hypothesis.

In humans, prenatal hypoxia (PH) is one of the most common adverse conditions in pregnancy. An ever-increasing amount of research has demonstrated that PH could affect the development and function of many organs, including the heart,[10] lung,[11] kidney,[12] liver[13] and brain,[14–16] eventually lead to the pathogenesis of many chronic diseases in adults. The brain is particularly vulnerable to hypoxia, and a growing body of evidence in humans and animals suggests that PH can result in aberrant hippocampus formation and function in offspring, leading to cognitive impairment and neurological disorders.[16–18] However, the mechanism by which PH causes cognitive impairment in offspring is still not fully understood.

Previous researches have revealed that cognitive failure is closely associated with synaptic malfunction or a lower number of synapses,[19–21] but the precise biochemical process underlying these alterations remains obscure. Cerebellin 1 (Cbln1) is abundantly expressed in granule cells of the cerebellum and is essential for cerebellar synaptic integrity and plasticity.[22] After release from parallel fibers (PFs), Cbln1 will bind to its postsynaptic receptor, glutamate receptor delta2 (GluD2), and plays a crucial role at PF-Purkinje cell synapses. Prior research has

[1]Institute for Fetology, The First Affiliated Hospital of Soochow University, Suzhou City, Jiangsu, China
[2]Department of Obstetrics and Gynecology, The First Affiliated Hospital of Anhui Medical University, Hefei, China
[3]Department of Gynaecology, Qingdao Hospital, University of Health and Rehabilitation Sciences (Qingdao Municipal Hospital), Qingdao, Shandong, China
[4]Center for Medical Genetics and Prenatal Diagnosis, Key Laboratory of Birth Defect Prevention and Genetic, Medicine of Shandong Health Commission, Key Laboratory of Birth Regulation and Control Technology of National Health Commission of China, Shandong Provincial Maternal and Child Health Care Hospital Affiliated to Qingdao University, Jinan, Shandong, China
[5]Dushu Lake Hospital Affiliated to Soochow University, Suzhou, Jiangsu Province, China
[6]These authors contributed equally
[7]Lead contact
*Correspondence: miaosunsuda@163.com
https://doi.org/10.1016/j.isci.2023.108703

demonstrated that Cbln1 is primarily responsible for cerebellar function.[23] It has been shown, however, that Cbln1 signaling is also engaged in non-motor processes in adult mice. For example, Otsuka et al. found that Cbln1 in the forebrain and cerebellum mediated specific aspects of fear conditioning and spatial memory, respectively.[24] Meanwhile, numerous studies have validated that *Cbln1* mRNA was also expressed outside the cerebellum,[24,25] suggesting that Cbln1 may also play a pivotal role in other brain regions. Above all, despite its major role in motor coordination and learning, it is unknown whether and how Cbln1 regulates cognitive functioning, particularly in the PH model.

Epigenetic dysregulation, which modifies gene expression in the brain, is suggested as one of the critical pathophysiology underpinnings of aging and neurodegeneration. N6-methyladenosine (m^6A) is the most prevalent internal epigenetic modification of eukaryotic mRNA, and is responsible for maintaining the stability of mammalian mRNA.[26] The brain contains very rich m^6A modifications, and studies have confirmed that m^6A alterations are intimately linked to neurodevelopmental and neuropsychiatric diseases.[27–29] In mammalian cells, m^6A is generated in the nucleus by METTL3/METTL14/WTAP, a multicomponent methyltransferase complex, and is removed by demethylase FTO and/or ALKBH5.[30] At the present, the molecular mechanisms of how m^6A exerts its regulatory functions on mRNA metabolism in species ranging from yeast to mammals are still poorly understood. Accumulating evidence suggests that m^6A primarily affects the stability,[31] splicing,[32] or translation[33] of the modified RNA mainly by recruiting particular m^6A reader proteins. The YTH domain-containing proteins (such as YTHDF1, YTHDF2, and YTHDF3) were the first m^6A reader proteins discovered[34] and provided a mechanistic basis for understanding the effects of m^6A in mRNA metabolism. Although some studies revealed a unified model of m^6A function in which all m^6A-modified mRNAs are subjected to the combined action of YTHDF proteins,[35] previous studies reported that each of the three YTH domain-containing proteins has a different effect on m^6A-containing mRNAs: YTHDF1 promotes translation, YTHDF2 promotes degradation, and YTHDF3 functions in both ways.[31,33,36] Therefore, given the association of m^6A modifications with various neurological diseases, it is warranted to investigate whether the YTH domain-containing proteins have been altered in the brain of PH model, as well as their role in the fate regulation of the nervous system function-related genes.

The stability of mRNA has emerged as a crucial aspect of eukaryotic gene expression regulation. Usually, eukaryotic mRNAs are protected by a 5′-cap structure and a 3′-poly-adenine (poly(A)) tail. Upon receiving a degradation signal, the RNA molecule follows one of the subsequent processes: the deadenylation-dependent decay pathway that starts with the shortening of the poly(A) tail and with the removal of the 5′-cap structure and the endonuclease-mediated decay pathway that is initiated by internal cleavage of the RNA or ARE (AU-rich element in 3′ UTR) sequence-dependent mRNA decay pathway.[37] Among these pathways, the vast majority of mRNAs in eukaryotes were subjected to the deadenylation-dependent degradation process. The molecules involved in the deadenylation-dependent decay pathway mainly include the carbon catabolite-repression 4-Not (CCR4-NOT) deadenylase complex, the B cell translocation gene/transducer of ERBB2 (BTG/Tob) family and poly(A)-binding protein (PABPC).[38–40] Notably, the CCR4-NOT deadenylase complex and the BTG/Tob family also play a role in the degradation of m^6A-containing mRNAs. For instance, Du et al. reported that YTHDF2 is implicated in the degradation of m^6A-containing mRNAs by the direct recruitment of the CCR4-NOT deadenylase complex.[41] Moreover, molecules involved in deadenylation-dependent decay pathways sometimes need to act synergistically. A previous study has demonstrated that the deadenylase activities of both Caf1 and its CCR4 partner are required for BTG2-induced poly(A) degradation.[42] The aforementioned findings demonstrate that deadenylation is essential for the regulation of gene expression. In addition, plentiful studies have illustrated that deadenylation-related molecular changes are associated with the occurrence of neurological diseases.[43,44] Therefore, the changes in the deadenylation-dependent decay pathway in the PH model and its roles in the development of cognitive impairment require further investigation.

In this study, we evaluated the cognitive function in the offspring of the PH group and explored the role of the m^6A pathway in this process. We present evidence that YTHDF3 is involved in the deadenylation-dependent decay of *Cbln1* mRNA by directly interacting with the BTG2, ultimately resulting in the decrease of Cbln1. Reduced expression of Cbln1 could lead to impaired synaptic function, potentially contributing to cognitive deficits in the offspring.

RESULTS

Impaired spatial learning and memory in PH offspring

The PH model was generated by placing pregnant mice into a chamber with reduced oxygen concentration at 10.5% from GD 12.5 to GD 17.5. Since intrauterine hypoxia can lead to intrauterine growth restriction, the birth weight of the offspring can be used to reflect whether the PH model is successfully established. As shown in Figure 1A, the birth weight of newborns in the PH group reduced dramatically ($p < 0.001$), indicating that the PH model was successfully constructed. In order to determine the link between PH and cognitive function, we assessed spatial learning and memory in the offspring via MWM tests. The male offspring in the PH group showed longer latency to the platform than the Ctrl group despite showing normal athletic ability (Figures 1B and 1C, $p < 0.05$; Figures S1A–S1D), suggesting that their spatial learning was impaired. In the space probe trial, offspring in the PH group failed to remember the platform location and exhibited fewer platform crossings (Figures 1D and 1F, $p < 0.01$) and less time spent in the target quadrant (Figures 1E and 1F, $p < 0.001$), indicating spatial memory deficits.

Moreover, to further confirm the relationship between PH and the learning and memory of the offspring, we performed step-through tests and NOR text. The results of the step-through test revealed that offspring in the PH group have more error times than offspring in the Ctrl group (Figure 1G, $p < 0.01$), suggesting defects in memory acquisition, although spending the same amount of time reaching the dark chamber for the first time (Figure 1H). Consistent with the preceding findings, offspring in the PH group spend less time exploring new objects than the Ctrl group during NOR testing (Figure 1I, $p < 0.05$). The findings presented above provide some support for the hypothesis that PH exposure is associated with cognitive deficits in the offspring, but the underlying mechanism needs more investigation.

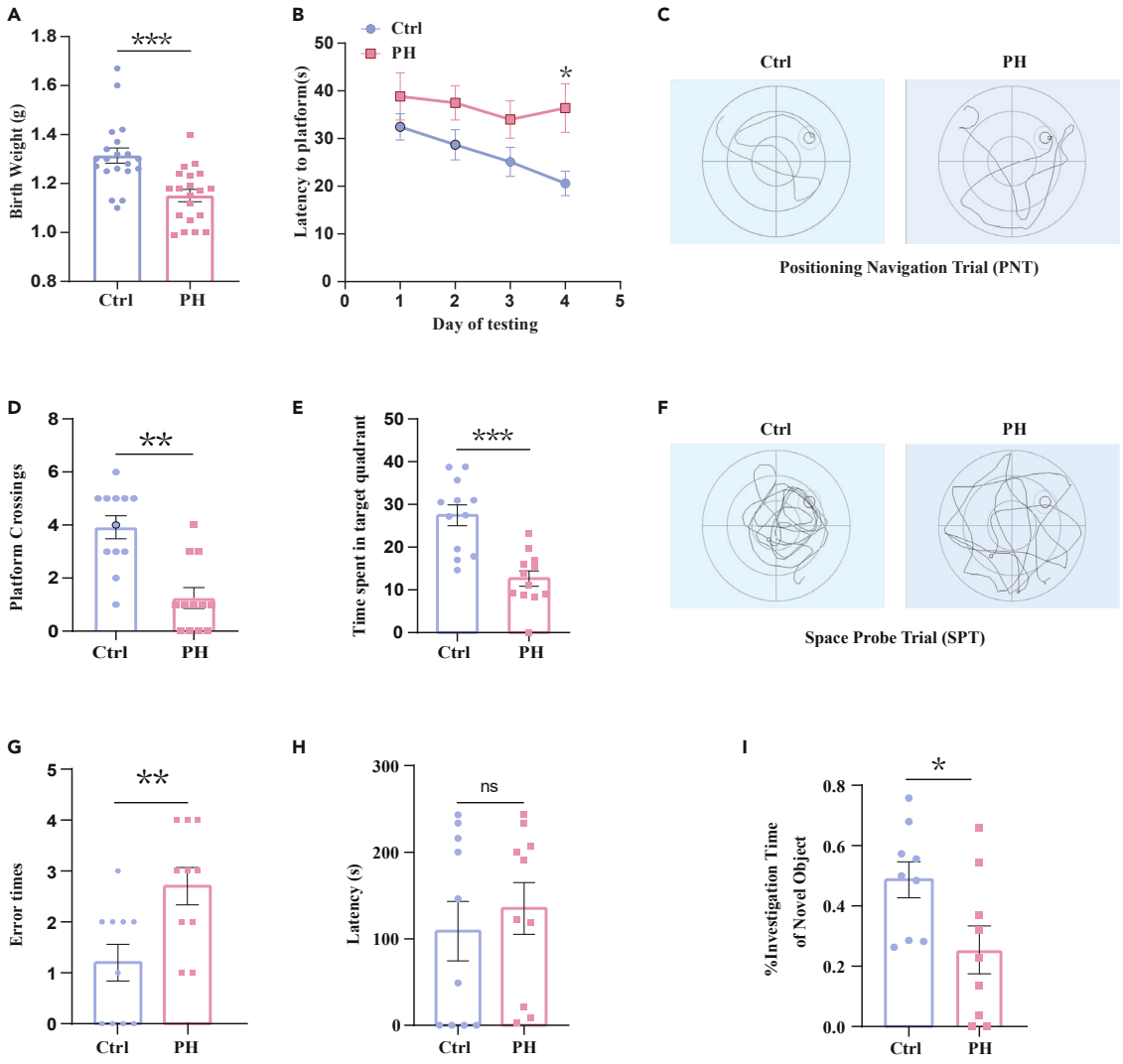

Figure 1. Impaired spatial learning and memory in PH offspring

(A) Birth weight between the two groups (Ctrl, n = 20; PH, n = 20).

(B) Learning curves of Ctrl (black, n = 12) and PH (red, n = 12) offspring in MWM tests with hidden platform.

(C) Representative swimming paths of Ctrl and PH offspring in the positioning navigation trial of MWM test.

(D) Platform crossing number of two groups (Ctrl, n = 12; PH, n = 12) in MWM probe test.

(E) Target quadrant time of two groups (Ctrl, n = 12; PH, n = 12) in the MWM probe test.

(F) Representative swimming paths of Ctrl and PH offspring in MWM probe test.

(G) Error times during the retention trial in step-through tests (Ctrl, n = 10; PH, n = 10).

(H) The time that mice in two groups (Ctrl, n = 10; PH, n = 10) took before initially entering the dark chamber (the step-through latency).

(I) Time exploring novel object during the test session (percentage) in NOR tests (Ctrl, n = 9; PH, n = 9). Data are shown as mean ± SEM. *, $p < 0.05$; **, $p < 0.01$; ***, $p < 0.001$; ns, no significance.

Impact of PH on synaptic function-related genes

In the mouse brain, the hippocampus is a crucial area for spatial learning and memory. Nissl staining was used to determine the number of hippocampus neurons. Qualitative analysis of Nissl staining results revealed notably fewer Nissl-stained neurons in the hippocampus of PH offspring compared to Ctrl offspring (Figures S1E and S1F, $p < 0.05$), indicating neuronal impairment in the offspring exposed to PH, and this may lead to cognitive impairment in offspring. In addition, the densities of dendritic spines were notably lower in PH offspring than in Ctrl offspring (Figures S1G and S1H, $p < 0.05$), also suggesting a potential alteration in neuron functions. To systemically investigate the mechanism underlying the cognitive impairment in prenatal hypoxia, we performed RNA sequencing (RNA-seq) analysis on Ctrl and PH offspring. We found that prenatal hypoxia had profound effects on the gene expression landscape in the hippocampus (Figure 2A). Intriguingly, the majority of differentially expressed genes (DEGs) were down-regulated and were enriched in synaptic transmission and synaptic plasticity

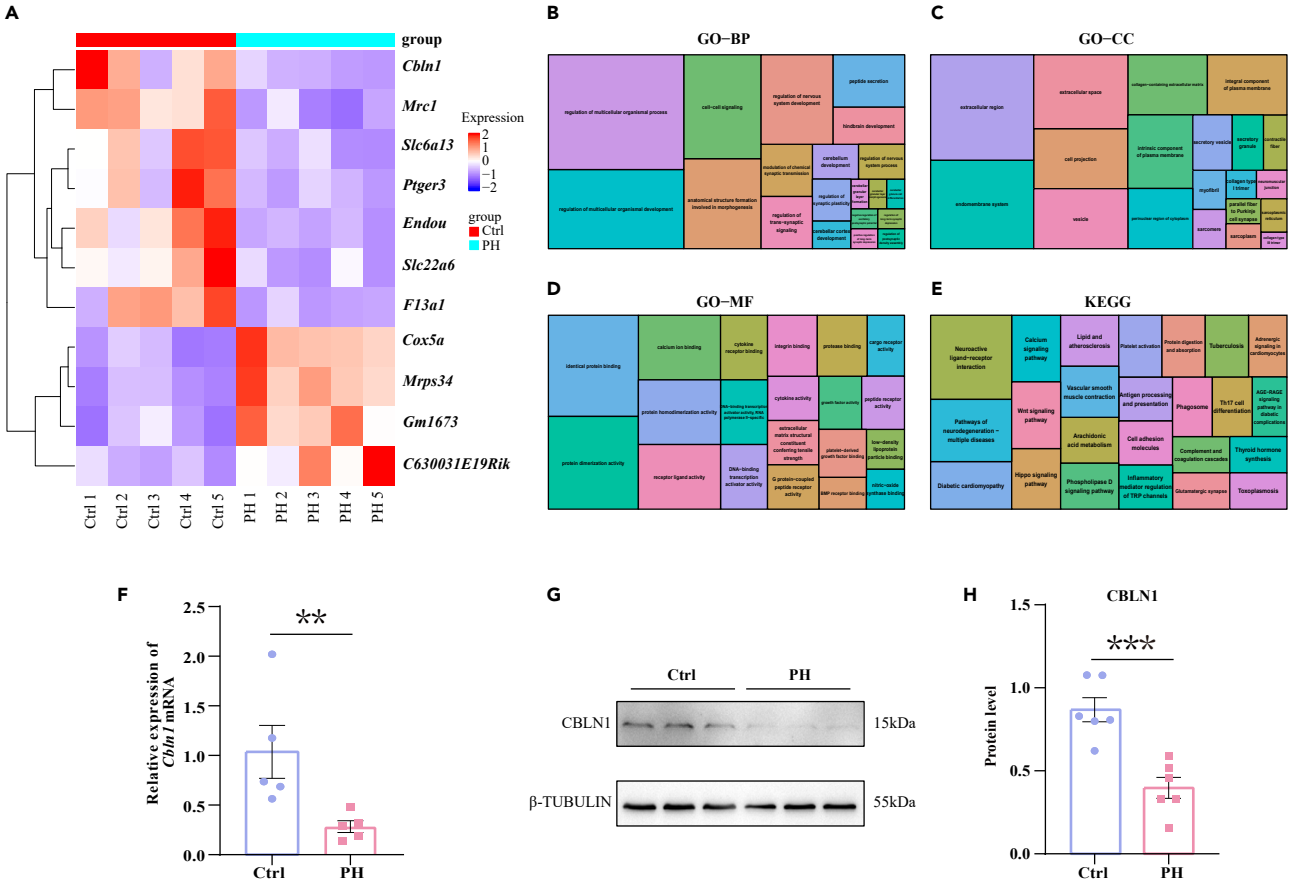

Figure 2. Impact of prenatal hypoxia on the gene expression landscape in the hippocampus

(A) Heatmap shows differentially expressed genes (DEGs) between the Ctrl and PH groups.

(B) Treemap of gene ontology (GO) Biological Process (BP) terms for DEGs, with the size of boxes corresponding to the number of DEGs associated with the GO category.

(C) Treemap of GO Cellular Component (CC) terms for DEGs, with the size of boxes corresponding to the number of DEGs associated with the GO category.

(D) Treemap of GO Molecular Function (MF) terms for DEGs, with the size of boxes corresponding to the number of DEGs associated with the GO category.

(E) Treemap of Kyoto Encyclopedia of Genes and Genomes (KEGG) terms for DEGs, with the size of boxes corresponding to the number of DEGs associated with the KEGG category.

(F) The mRNA level of *Cbln1* in the hippocampus from two groups (Ctrl, n = 5; PH, n = 5).

(G and H) The protein level of CBLN1 in the hippocampus from two groups (Ctrl, n = 6; PH, n = 6). Data are shown as mean ± SEM. **, $p < 0.01$; ***, $p < 0.001$.

(Figures 2B–2E). Further analysis revealed that the *Cbln1* gene (traditional synapse organizer) declined most dramatically among DEGs in response to PH, and RT-qPCR corroborated the down-regulation of the *Cbln1* gene (Figure 2F, $p < 0.01$), which further validated the reliability of transcriptome-wide RNA-seq data. Consistent with the transcriptional changes, the protein level of CBLN1 was also reduced in PH offspring (Figures 2G and 2H, $p < 0.001$).

Given that the *Cbln1* gene is essential for synaptic function, we evaluated the synaptic markers SYN and PSD95 in the hippocampus of offspring in two groups to determine whether PH altered synapse formation. As shown in Figures 3A–3C, both PSD95 and SYN levels were significantly decreased in PH offspring than in Ctrl offspring, suggesting abnormal synaptic function upon PH condition. Previous studies have shown that abnormal cognitive function is strongly associated with synaptic dysfunction or decreased synapse number.[19–21] The above results suggest that the cognitive impairment of offspring in the PH group may be related to abnormal synaptic function in the hippocampus, however, the underlying mechanism needs to be further explored.

YTHDF3 up-regulated in PH offspring

Epigenetic modifications influence gene expression in the brain and are a crucial pathophysiological basis of aging and neurodegenerative disorders. Among them, m^6A is the most common reversible modification inside eukaryotic mRNA, which mainly regulates gene expression by affecting the metabolism of mRNA. A large number of studies have shown that the brain is rich in m^6A modification, and the change of m^6A modification is closely related to neurodevelopment and neuropsychiatric diseases.[27–29] Consequently, we hypothesize that PH may lead to

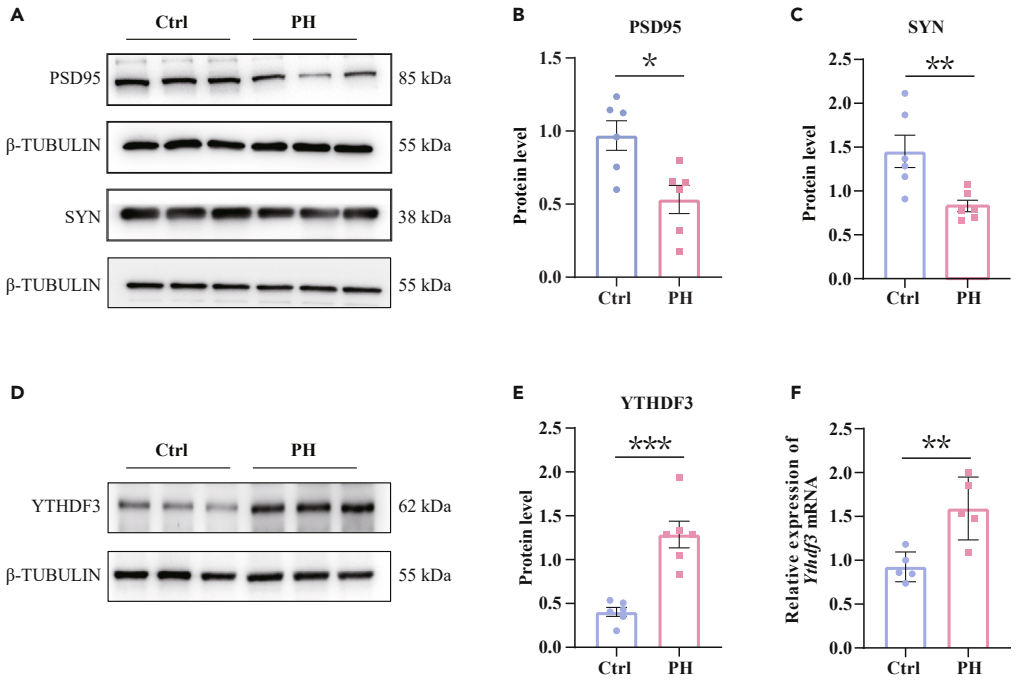

Figure 3. Hypoxia-induced reduced synaptic function *in vivo*

(A, B, and C) The protein level of PSD95 and SYN in the hippocampus from two groups (Ctrl, n = 6; PH, n = 6).

(D and E) The protein level of YTHDF3 in the hippocampus from two groups (Ctrl, n = 6; PH, n = 6).

(F) *Ythdf3* mRNA expression in the hippocampal tissues from two groups (Ctrl, n = 5; PH, n = 5). Data are shown as mean ± SEM. *, $p < 0.05$; **, $p < 0.01$; ***, $p < 0.001$.

alterations in m^{6}A modification in the hippocampus, thereby influencing the expression of cognition-related genes and resulting in cognitive impairment in offspring. In this study, we examined the expression of genes involved in the m^{6}A regulation by RT-qPCR (Figures S2A–S2H). Results indicated that both the protein (Figures 3D and 3E, $p < 0.001$) and mRNA (Figure 3F, $p < 0.01$, Figure S2H, fold change >1.5) level of YTHDF3 were significantly increased in the PH group compared to the Ctrl group, suggesting that YTHDF3 may contribute to the cognitive impairment upon PH condition. However, it remains to be determined whether YTHDF3 is involved in regulating the expression of cognition-related genes and synaptic function during PH.

Co-regulation of YTHDF3 and CBLN1 induced by hypoxia *in vitro*

In order to confirm the association between hypoxia and synaptic function, N2a cells were treated with 3% O_2 for 12 h in the chamber to mimic the context of hypoxia *in vitro*. Consistent with the results mentioned above, the protein level of CBLN1 (Figures 4A and 4B, $p < 0.05$) was reduced significantly in the hypoxia (HY) group compared with the control (Ctrl) group, while the protein level of YTHDF3 was up-regulated in the HY group than in the Ctrl group (Figures 4A and 4C, $p < 0.01$). Moreover, as shown in Figures 4D–4F, the synaptic markers PSD95 and SYN were decreased both in protein level ($p < 0.01$ and $p < 0.01$, respectively) and mRNA level ($p < 0.05$ and $p < 0.05$, respectively) in the HY group than in the Ctrl group. These results are consistent with the observed changes *in vivo*. Apart from this, to investigate the roles of CBLN1 in synaptic function, we knocked down the *Cbln1* in N2a cells and found that synaptic markers PSD95 and SYN decreased significantly (Figures 4G–4I, $p < 0.01$), illustrating that CBLN1 might play an important role in synaptic function. Combined with the most obvious down-regulation of *Cbln1* gene expression in the hippocampus, we speculate that the change of *Cbln1* expression has a strong correlation with the generation of offspring phenotypes. Therefore, the molecular mechanism underlying the altered expression of the *Cbln1* gene will be investigated later in discussion.

m^{6}A-methylomes in two groups

To gain more insight into the role of m^{6}A in regulating genes related to synaptic function, we first examined whether the m^{6}A levels changed under PH condition. Dot blot assay revealed reduced m^{6}A abundance in the hippocampus of the PH offspring compared with Ctrl offspring (Figure 5A). Then we performed the MeRIP-seq in two groups. As shown in Figure 5B, the m^{6}A sites were significantly enriched at start codons, CDS, stop codons, and 3′ UTRs in two groups. This is consistent with previous reports,[45] indicating that the sequencing results are very reliable. In addition, the highly overrepresented m^{6}A RRACH (R = G/A, H=U/A) motif identified using the HOMER algorithm in both PH group and Ctrl group further proved the successful enrichment of m^{6}A-modified mRNA (Figure 5C), because RRACH motif is also the most common conserved motif in the m^{6}A modified region.[46] To understand the function of m^{6}A in the brain, we performed gene ontology (GO) enrichment analysis on mRNAs with

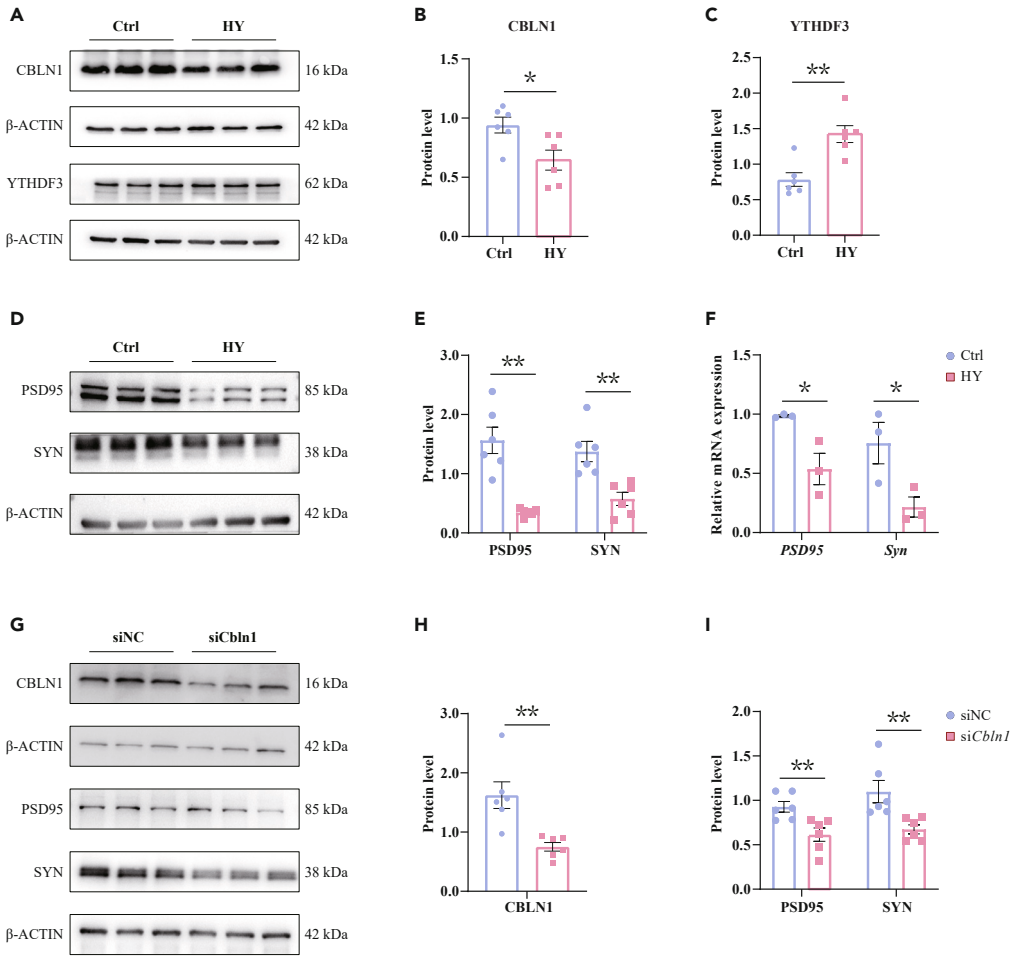

Figure 4. Co-regulation of YTHDF3 and CBLN1 induced by hypoxia in vitro

(A, B, and C) Protein level of CBLN1 and YTHDF3 in N2a cells after being treated with 3% O_2 for 12 h (Ctrl, n = 6; HY, n = 6).

(D and E) Protein level of PSD95 and SYN in the N2a cells after treatment with 3% O_2 for 12 h (Ctrl, n = 6; HY, n = 6).

(F) *PSD95,* and *Syn* mRNA expression in the N2a cells after being treated with 3% O_2 for 12 h (Ctrl, n = 3; HY, n = 3).

(G, H, and I) Representative western blots result of PSD95 and SYN from *Cbln1* knockdown N2a cells (siNC, n = 6; si*Cbln1*, n = 6). Data are shown as mean ± SEM. *, $p < 0.05$; **, $p < 0.01$.

different level m^{6}A-containing peaks in two groups and found that they were involved in various processes, including nervous system development, neuron to neuron synapse and postsynaptic specialization (Figure 5D). In addition, further Kyoto Encyclopedia of Genes and Genomes (KEGG) analysis indicated that differed m^{6}A-modified mRNAs were enriched in glutamatergic synapse and axon guidance pathways (Figure 5E). And interestingly, the m^{6}A-containing peak of *Cbln1* mRNA shrank remarkably in PH group compared with the Ctrl group (Figure 5F), and the m^{6}A sites were located at the 3′UTR of *Cbln1* mRNA, suggesting that m^{6}A modification may contribute to the regulation of *Cbln1* expression.

Cbln1 is an important target gene of YTHDF3

Given that m^{6}A may contribute to the regulation of *Cbln1* expression, we investigated whether YTHDF3 (a known m^{6}A reader) can regulate *Cbln1* expression levels by recognizing m^{6}A sites on *Cbln1* mRNA using the RNAct database (http://rnact.crg.eu/). We identified many genes (namely YTHDF3-binding genes) that can interact with the YTHDF3 protein. Interestingly, the *Cbln1* gene is the only one overlapping between YTHDF3-binding genes and DEGs in RNA-seq (Figure S3A), which strongly suggests the interaction between YTHDF3 protein and *Cbln1* mRNA. This result was further confirmed by RIP-qPCR, as we found that YTHDF3 was especially associated with *Cbln1* transcripts in the hippocampus (Figures 5G and 5H, $p < 0.01$).

To further investigate the association between YTHDF3 and *Cbln1* gene, N2a cells were transfected with *Ythdf3* siRNA. After 48 h, the protein was isolated for immunoblot analysis. We first determined the efficiency of gene knockdown by immunoblot analysis. As shown in Figures 6A and 6B ($p < 0.05$), the protein level of YTHDF3 was significantly reduced when the N2a cells were transfected with *Ythdf3* siRNA. And then, we found that knockdown of *Ythdf3* substantially increases the protein level of CBLN1 (Figures 6A and 6C, $p < 0.05$), PSD95

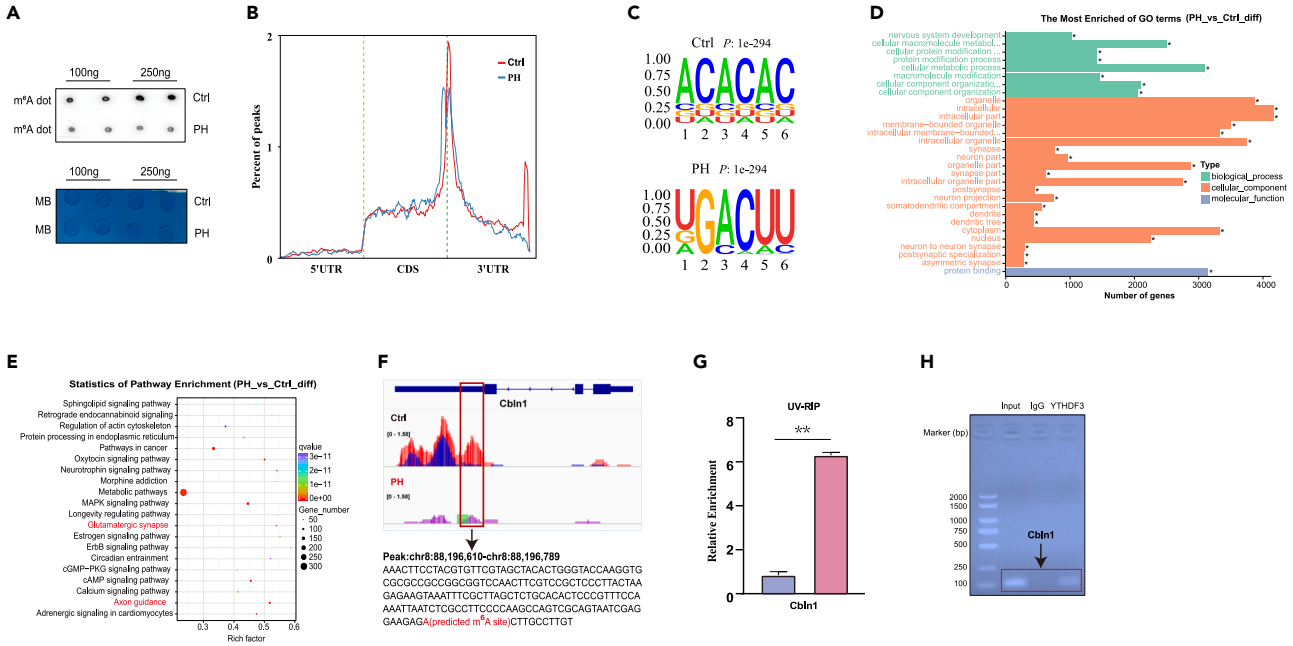

Figure 5. *Cbln1* is an important target gene of YTHDF3

(A) Representative dot blot images showing m^{6}A abundance in two groups.

(B) Distribution of high-confidence m^{6}A-containing peaks across the length of mRNA in two groups (Ctrl, red line; PH, blue line).

(C) Binding motif identified by HOMER with m^{6}A-containing peaks in two groups.

(D) Representative Gene Ontology (GO) terms of the biological process, cellular component, and molecular function categories enriched in transcripts with different m^{6}A-containing peaks. Gene ontology (GO) analysis was performed using the DAVID bioinformatics database. GO classification for cellular component, biological process, and molecular function were performed with default settings.

(E) Bubble chart for representative Kyoto Encyclopedia of Genes and Genomes (KEGG) terms enriched in transcripts with different level m^{6}A-containing peaks.

(F) m^{6}A abundance on *Cbln1* mRNA in Ctrl or PH hippocampus was plotted by the IGV. Blue and purple colors show the m^{6}A signals of input samples from two groups, while red and green stand for signals of IP samples from two groups. The range of signals in all groups was normalized to a 0–1.58 scale. At the same position, the m^{6}A peaks of the IP group over the input group were recognized as the genuine m^{6}A level. Blue blocks above indicated the sites where the m^{6}A level differed between two groups (the nucleotide sequence of the m^{6}A level differed regions were shown later in discussion), and the most remarkable location were highlighted with a scarlet pane.

(G) Relative enrichment of *Cbln1* mRNA associated with YTHDF3 protein was identified by UV-RIP assays using anti-IgG and anti-YTHDF3 antibodies. The IgG group was a negative control to preclude nonspecific binding. Data are shown as mean ± SEM, n = 2.

(H) Agarose gel electrophoresis results by using RT-qPCR products from UV-RIP assays. The product (Cbln1) location was highlighted with a red dotted box. Data are shown as mean ± SEM. **, $p < 0.01$.

(Figures 6D and 6E, $p < 0.05$), and SYN (Figures 6D and 6F, $p < 0.05$). Moreover, the *Cbln1* mRNA expression was upregulated after the knockdown of YTHDF3 (Figure 6G, $p < 0.01$). These results imply that YTHDF3 regulates the expression of *Cbln1* gene and may affect its fate determination in cells, and is critical for regulating synaptic function. In contrast, overexpression of *Ythdf3* could lead to a remarkable decrease in the expression of CBLN1, PSD95, and SYN (Figure S4).

It is well established that YTHDF3, a well-known m^{6}A reader, may play a critical role in accelerating the metabolism of m^{6}A-containing mRNAs.[36] Accordingly, we performed an mRNA stability assay to measure the half-life of *Cbln1* mRNA after the knockdown of *Ythdf3*. Interestingly, the knockdown of *Ythdf3* stabilized the *Cbln1* transcripts (Figure 6H, $p < 0.01$), suggesting that YTHDF3 may partly regulate the expression of *Cbln1* at the transcriptional level by destabilizing the *Cbln1* transcripts, however, the specific molecular mechanism needs to be further explored.

YTHDF3 regulates *Cbln1* mRNA stability in an m^{6}A-dependent manner

Combining analysis of our MeRIP-seq data (Figure 5E) with the potential m^{6}A sites of the *Cbln1* gene predicted by the SRAMP database (http://www.cuilab.cn/sramp, Figure S3B and S3C), we identified a very high-confidence m^{6}A site (location at chr8: 88,196,620, GRCm39/mm39) in the 3′UTR of *Cbln1* transcript. Moreover, this site shows remarkable conservation across species (Figure 7A). Hence, we construct a luciferase reporter gene by inserting the 3′UTR sequence, which was shown in Figure 5E, into the pmirGLO vector (Figure 7B). *Cbln1*-3′UTR mutant was directly synthesized by replacing the A (Adenosine) with C (Cytosine) in the m^{6}A motif (Figure 7C). Additionally, we found that overexpression/knockdown of *Ythdf3* had no effect on the mutant *Cbln1*-3′UTR luciferase activity (Figures 7D and 7E) but had a significant impact on the wild-type *Cbln1*-3′UTR luciferase activity (Figures 7D and 7E, $p < 0.01$ and $p < 0.01$, respectively). These data indicate that YTHDF3 regulates *Cbln1* expression through an m^{6}A-dependent manner.

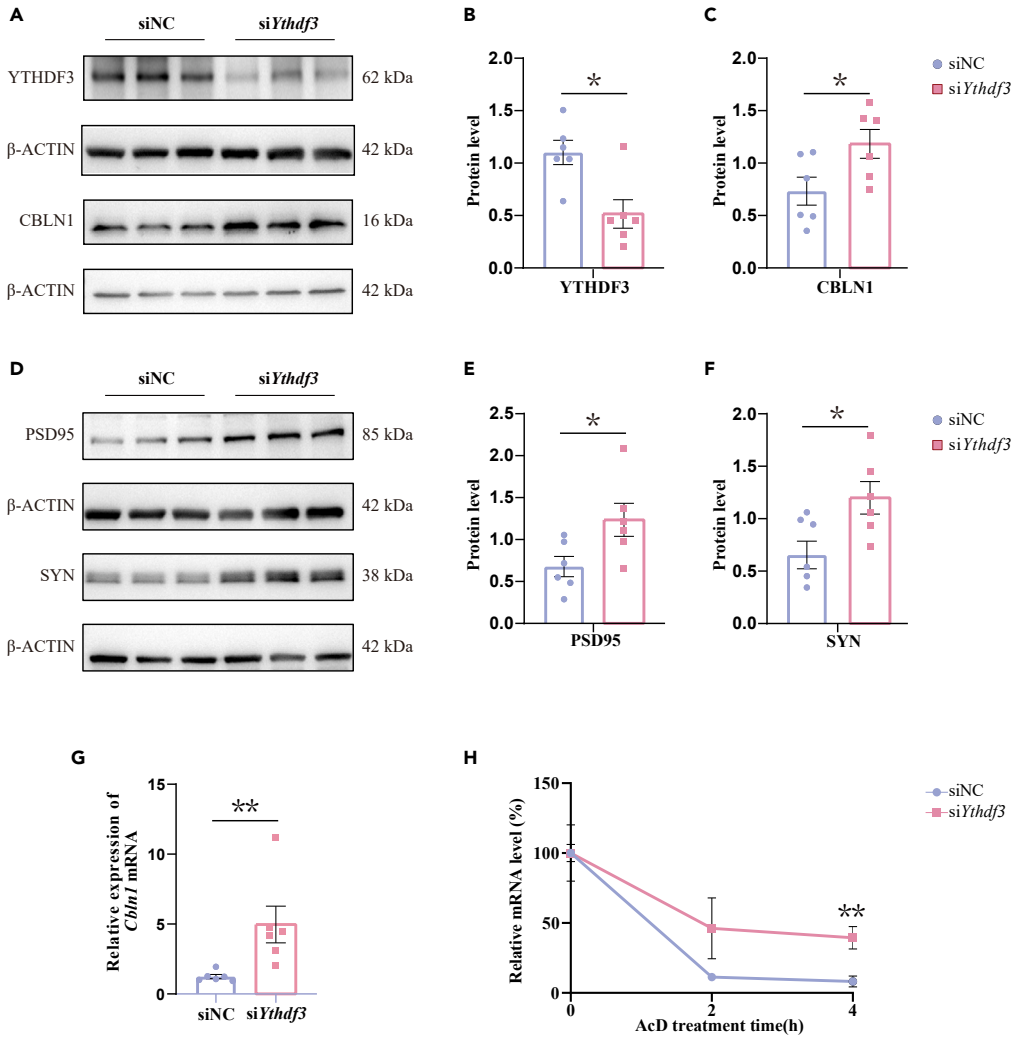

Figure 6. YTHDF3 determines *Cbln1* fate by regulating transcript stability *in vitro*

(A, B, and C) Western blot was performed to analyze the level of YTHDF3 and CBLN1 in the N2a cell line after treatment with si*Ythdf3*. siNC, negative control, n = 6; si*Ythdf3*, *Ythdf3* knockdown, n = 6.

(D, E, and F) Representative western blots result of PSD95 and SYN from *Ythdf3* knockdown N2a cells. siNC, negative control, n = 6; si*Ythdf3*, *Ythdf3* knockdown, n = 6.

(G) RT-qPCR results of *Cbln1* expression from *Ythdf3* knockdown N2a cells. siNC, negative control, n = 6; si*Ythdf3*, *Ythdf3* knockdown, n = 6.

(H) Representative mRNA profile of *Cbln1* at 0-, 2-, and 4-h time points after actinomycin D (5 μg/mL) treatment (h.p.t.) in NC (negative control, n = 6) and si*Ythdf3* (*Ythdf3* knockdown, n = 6) group. Data are shown as mean ± SEM. *, $p < 0.05$; **, $p < 0.01$.

YTHDF3 destabilizes *Cbln1* mRNA by recruiting BTG2

As a m^{6}A reader, YTHDF3 can regulate the stability of *Cbln1* mRNA when it binds to the m^{6}A modification site on *Cbln1* mRNA. However, YTHDF3 may not directly induce mRNA degradation; therefore, the mechanism of how YTHDF3 regulates the stability of *Cbln1* mRNA requires more investigation. Given that the deadenylation-dependent decay pathway is a predominant way of regulating mRNA stability. Then we examined the expression of molecules participating in deadenylation pathway *in vivo* and *in vitro*, and the results showed that the mRNA expression of *Cnot4, Cnot7*, *Btg1* and *Btg2* notably increased in the hippocampus of PH offspring compared with the Ctrl offspring (Figures 8A and 8B). Because study has shown that CNOT7, BTG1 and BTG2 can form a complex and play a role in regulating gene expression,[47] so follow-up experiments mainly focus on *Cnot7*, *Btg1* and *Btg2* genes. Additionally, consistent with the results *in vivo*, the mRNA level of *Btg1* and *Btg2* also increased significantly in N2a cells treated with 3% O_2 (Figure 8C, $p < 0.05$ and $p < 0.01$, respectively). However, the mRNA level of *Cnot7* remained unchanged. Moreover, immunoblot analysis confirmed that the protein level of BTG2 increased significantly in PH offspring than in Ctrl group (Figures 8D and 8E, $p < 0.05$), while the protein level of CNOT7 remained unchanged (Figures 8D and 8F). Regrettably, due to the poor quality of the BTG1 antibody, the results are not shown. Therefore, we investigated the role of BTG2 in the regulation of *Cbln1* mRNA stability.

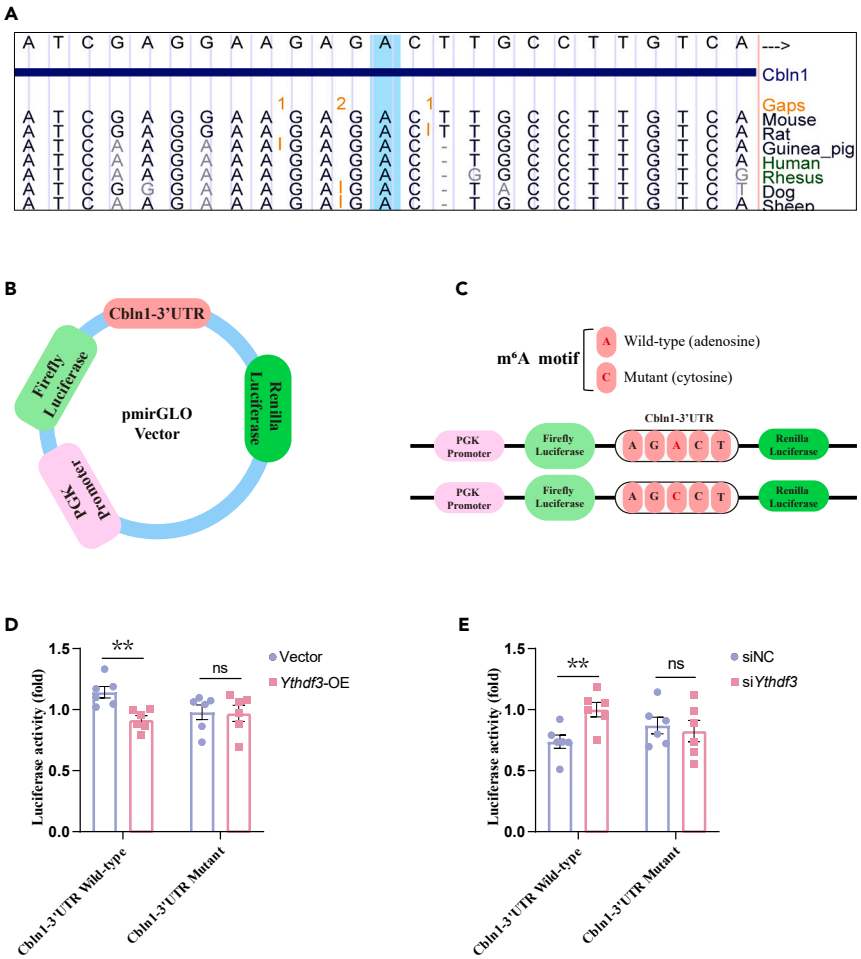

Figure 7. YTHDF3 regulates *Cbln1* mRNA stability in an m^{6}A-dependent manner

(A) Conservation of a very high-confidence m^{6}A site in the 3′UTR of *Cbln1* transcript, and the m^{6}A site location was highlighted with a sky blue background.

(B and C) Graphical explanation for the construction of luciferase reporters. The wild-type or mutant (m^{6}A motif mutated) sequence of Cbln1-3′UTR was inserted into a pmirGLO vector between Firefly and Renilla elements. Relative luciferase activity was computed by the ratio of Firefly and Renilla luciferase values.

(D and E) Relative luciferase activity of N2a cells transfected with the Cbln1-wild type or -mutated construct was measured, with normal or altered the expression of *Ythdf3*. Data are shown as mean ± SEM. **, $p < 0.01$; ns, no significance.

Previous study has shown that the m^{6}A reader protein YTHDF2 can participate in the degradation of m^{6}A-modified mRNA by directly recruiting the CCR4-NOT deadenylase complex.[41] Therefore, to explore the molecular mechanism by which YTHDF3 functions as a modulator of mRNA stability, we screened for the interaction between YTHDF3 and BTG2 using co-immunoprecipitation (co-IP) assays. As shown in Figure 8G, YTHDF3 co-immunoprecipitated with BTG2, suggesting that BTG2 may be responsible for the YTHDF3-mediated destabilization of *Cbln1* mRNA. In addition, further analysis demonstrated that the knockdown of BTG2 could partially inhibit the down-regulation of *Cbln1* expression caused by the overexpression of YTHDF3 (Figures 8H–8K), which further proves that BTG2 is essential for YTHDF3 to exert its regulatory function on *Cbln1* expression.

DISCUSSION

In the present study, by addressing the questions at the *in vivo*, cellular and molecular levels and the successful construction of the PH model, we provide a comprehensive approach to understanding the mechanisms linking m^{6}A modification to programmed synaptic dysfunction in offspring following PH. The data show that under PH conditions, YTHDF3 was significantly increased in the hippocampus of offspring in the PH group, and it regulated the stability of *Cbln1* mRNA by binding to the m^{6}A modification site on the *Cbln1* gene and further recruiting the deadenylation regulator BTG2, which eventually led to the down-regulation of *Cbln1* gene expression. CBLN1 deficiency can result in aberrant synapse function and subsequently cognitive impairment in PH-exposed offspring.

Human clinical studies and preclinical animal models support the notion that maternal stress during pregnancy can result in brain development issues in the fetus.[48,49] In humans, chronic fetal hypoxia is one of the most prevalent consequences of complicated pregnancy, and it may be

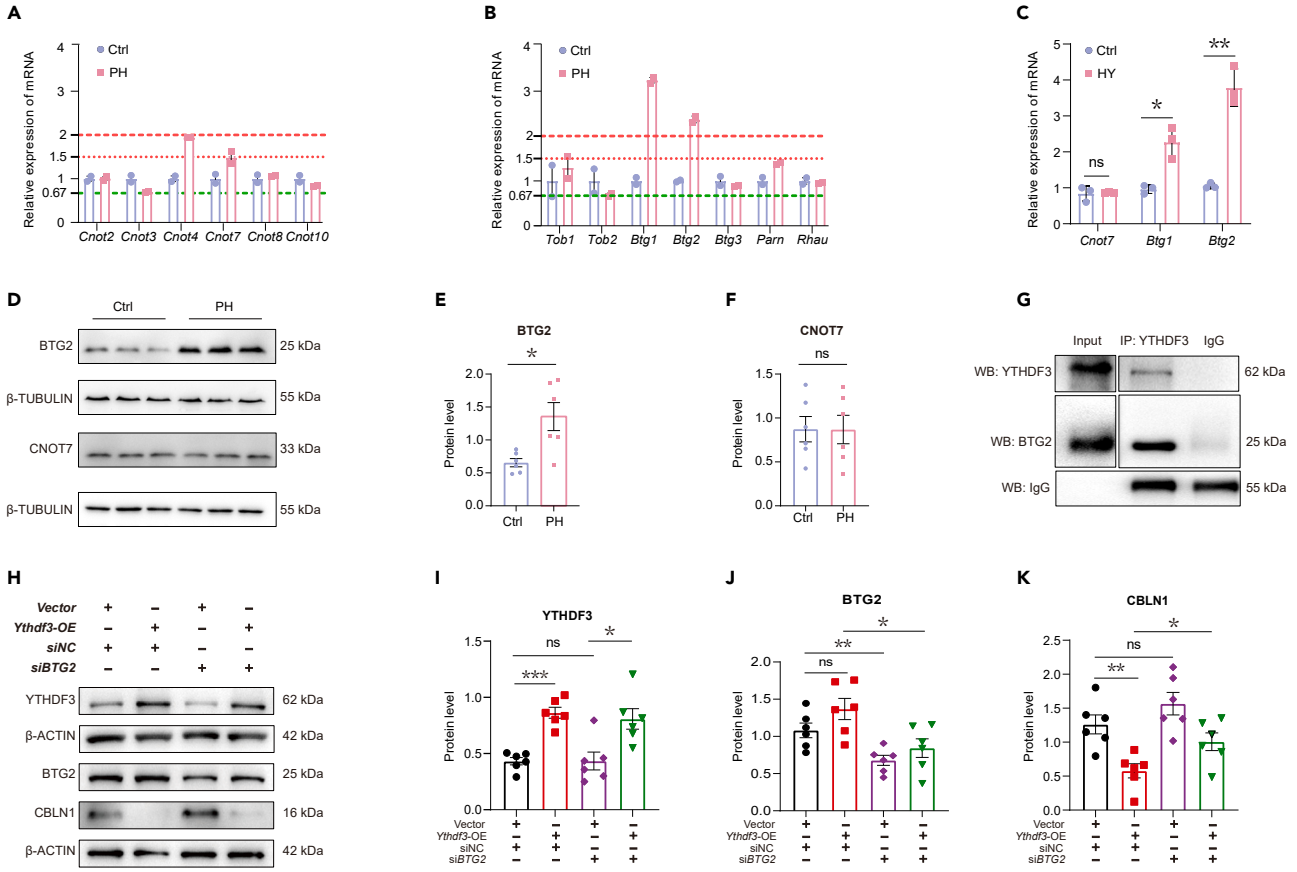

Figure 8. YTHDF3 destabilizes *Cbln1* mRNA by recruiting BTG2

(A and B) The expression levels of CCR4–NOT deadenylase complex (*Cnot2*, *Cnot3*, *Cnot4*, *Cnot7*, *Cnot8*, *Cnot10*), BTG/Tob family members (*Tob1*, *Tob2*, *Btg1*, *Btg2*, *Btg3*), *Parn* and *Rhau* in the hippocampus from two groups (Ctrl, n = 2; PH, n = 2).

(C) The expression levels of *Cnot7*, *Btg1*, and *Btg2* in N2a cells treated with 3% O_2 for 24 h (Ctrl, n = 3; HY, n = 3).

(D, E, and F) The protein level of BTG2 and CNOT7 in the hippocampus from two groups (Ctrl, n = 6; PH, n = 6).

(G) YTHDF3 antibody, and control IgG antibody were used for immunoprecipitation of the mouse hippocampal tissue. YTHDF3-interacting proteins were examined by western blotting with anti-BTG2. The representative images were shown.

(H, I, J, and K) The protein level of YTHDF3, BTG2, and CBLN1 in N2a cells after being treated with si*BTG2* and *Ythdf3*-OE. Data are shown as mean ± SEM. *, $p < 0.05$; **, $p < 0.01$; ***, $p < 0.001$; ns, no significance.

detrimental to the development and health of offspring.[50–53] Moreover, Shen et al. reported that antenatal hypoxia increased the susceptibility of Alzheimer's disease (AD) in the offspring of 5xFAD mice.[54] Similarly, we also discovered diminished cognitive performance in PH offspring through MWM, NOR, and step-through tests, however, the process requires further investigation. The hippocampus, which is required for spatial and episodic memory, is disrupted early in AD. Previous studies have demonstrated that the hippocampus is susceptible to the influence of hypoxia.[55,56] Therefore, chronic fetal hypoxia may contribute to the pathogenesis of cognitive impairment by damaging the function of the hippocampus. Later Nissl staining results showed that the Nissl bodies in the hippocampal tissue of offspring in the PH group were significantly reduced, indicating that PH can lead to hippocampal neuron damage in adult offspring, which may be related to the cognitive impairment of offspring.

Synapse loss has been shown to be strongly associated with the cognitive impairment phenotype of AD.[57,58] In this study, we consistently found that synaptic function-related molecules SYN and PSD95 decreased remarkably in the hippocampus of PH offspring through biological methods. These results suggest that hypoxia during pregnancy leads to abnormal synaptic function in the hippocampus. Importantly, previous studies have shown that adverse stress during pregnancy, including PH-induced synapse loss, is closely related to the occurrence of fetal or postnatal neurological diseases.[59,60] Moreover, in the present study, the hypoxic treatment was performed on the pregnant mice from the GD12.5 to the GD17.5, and this time window is a critical period of brain development (such as neurogenesis, synaptogenesis).[61] Thus, all of the above evidence suggests that PH leads to cognitive impairment in adult offspring, which is associated with the abnormal synaptic function in the hippocampus. However, the specific molecular biological mechanism of synaptic function loss needs to be further explored.

Previous studies suggested that Cbln1 has an essential effect on synaptogenesis and is necessary for maintaining normal synapses. Cbln1 dysfunction is sufficient to cause a severe reduction in the number of synapses.[62] Here, we found that *Cbln1* mRNA decreased significantly in the hippocampus of PH offspring via RNA-seq analysis and RT-qPCR. Although the functions of Cbln1 in the cerebellum have been described

extensively, more evidence suggests that Cbln1 has an impact on the hippocampal function. Otsuka et al. reported that spatial learning and fear conditioning were abrogated in forebrain-predominant Cbln1-null mice.[24] In addition, Seigneur et al. investigated the function of cerebellins (including Cbln1, Cbln2, and Cbln4) throughout the brain outside the cerebellum, they found that Cbln1/2 double KO (dKO) aging (6-month-old) mice exhibited an obvious decrease in hippocampal synapse density.[63] More interestingly, a lab from Keio university designed a synthetic synaptic organizer protein CPTX (containing structural elements from Cbln1), and found that CPTX can restore synaptic functions and spatial and contextual memories in mouse models for AD.[64] Notably, we found that synaptic markers PSD95 and SYN decreased significantly after the knockdown of *Cbln1*. These results indicated that Cbln1 is likely to contribute to the PH offspring's behavior deficits. However, the precise process responsible for the alteration of Cbln1 is not yet completely understood.

Although the FOAD concept has been largely accepted, the precise biological process underlying it remain elusive. Currently, the most well-known mechanism associated with FOAD hypothesis is the epigenetic mechanism, which is also regarded as the foundation of the FOAD hypothesis.[65–67] m^{6}A modification is the most common chemical modification found in eukaryotic mRNA in recent years.[68] Research have demonstrated that m^{6}A modification controls gene expression via influencing intracellular mRNA metabolism, including mRNA stability and translation.[69] Importantly, studies have shown that m^{6}A modification is highly enriched in the brain,[70,71] suggesting that it may play an important role in the nervous system. For example, accumulating evidence shows that m^{6}A modification is dramatically involved in the pathogenesis of multiple neurodevelopmental[29,72–74] and neuropsychiatric disorders,[75–78] including AD.[64,79,80] Previous studies suggested that m^{6}A-containing mRNA transcripts tend to be less stable after recognizing by m^{6}A reader YTHDF2 alone[81] or together with YTHDF3.[36] Here we found that the level of YTHDF3 increased significantly in PH offspring. Meanwhile, through high-quality MeRIP-seq analysis, we found that the m^{6}A peak of *Cbln1* in 3′UTR shrank remarkably in the hippocampus of PH offspring compared with Ctrl offspring, suggesting that *Cbln1* mRNA may be regulated by m^{6}A modification. The reasons for the differential methylation observed may including: 1) increased in m^{6}A eraser YTHDF3 which leads to increased Cbln1 degradation following hypoxia, and the decreased levels of mRNA may be accompanied by corresponding decreases in methylation levels; 2) Hypoxia can affect the methylation level by affecting the function of methylase or demethylase.[82,83] Therefore, we hypothesized that the reduction of Cbln1 might be due to the up-regulation of YTHDF3 in the PH model. Interestingly, Cbln1 was significantly increased in *Ythdf3* knockdown N2a cells *in vitro*. Meanwhile, SYN and PSD95 also increased in *Ythdf3* knockdown N2a cells. Further study showed that the stability of *Cbln1* transcript also increased in YTHDF3 deficiency N2a cells, suggesting that YTHDF3 serves to regulate the stability of *Cbln1* mRNA at the post-transcriptional level. Mechanistically, further analysis combing MeRIP-seq data and SRAMP database showed a conservative m^{6}A site in the 3′UTR of the *Cbln1* transcript. Dual-luciferase reporter assay showed an essential effect of this site in the process of YTHDF3-induced decay of *Cbln1* mRNA. The above results confirmed that the m^{6}A modification site in the 3′UTR region of the *Cbln1* gene is crucial for YTHDF3 to exert its regulatory effect, that is, YTHDF3 negatively regulates the expression of the *Cbln1* gene in an m^{6}A-dependent manner. However, as an m^{6}A reader protein, YTHDF3 may not directly lead to mRNA degradation, so the mechanism of how YTHDF3 regulates the stability of *Cbln1* mRNA needs further investigation.

A previous study has demonstrated that expedited poly(A) shortening is crucial for the decay of m^{6}A-containing RNAs, and deadenylases are responsible for accelerated deadenylation.[41] CCR4-NOT deadenylase complex and BTG/Tob family are the most critical members involved in regulating the deadenylation-dependent mRNA decay. For example, Du et al. discovered that YTHDF2 directly interacts with CNOT1 to destabilize m^{6}A-containing transcripts.[41] In addition, Liu et al. showed a parallel function of YTHDF2 and YTHDF3 for somatic reprogramming through different RNA deadenylation pathways.[84] In this study, we found that the level of BTG2 increased remarkably in the hippocampus of PH offspring and N2a cells treated with 3% O_2. Further investigation through co-immunoprecipitation analysis showed YTHDF3 co-immunoprecipitated with BTG2. Moreover, the knockdown of BTG2 can partially reverse the reduction of *Cbln1* gene expression by YTHDF3 overexpression. The above findings indicated that the deadenylation regulator BTG2 was involved in the regulation of *Cbln1* gene expression by YTHDF3.

In summary, our study found that YTHDF3 destabilizes *Cbln1* mRNA in an m^{6}A-dependent manner through direct interaction with BTG2. Cbln1 dysfunction-induced abnormal synaptic function may contribute to the cognition impairment of PH offspring. Our study links m^{6}A modifications with the post-transcriptional regulation of the *Cbln1* expression and provides a direction for finding effective therapeutic strategies for treating synaptic dysfunction caused by PH.

Limitations of the study

In addition, previous study has confirmed that YTHDF3 can also regulate the translation of mRNA.[85] However, this study focuses on the regulation of *Cbln1* mRNA stability by YTHDF3. Therefore, whether YTHDF3 regulates the translation of the *Cbln1* gene still needs further research.

This study found that BTG2 is involved in the regulation of Cbln1 gene expression by YTHDF3. However, as a deadenylation regulator, BTG2 needs to regulate the activity of deadenylation enzyme to finally exert its effect. Therefore, the mechanism by which YTHDF3 recruits BTG2 to exert its effect may still need further exploration.

STAR★METHODS

Detailed methods are provided in the online version of this paper and include the following:

- KEY RESOURCES TABLE
- RESOURCE AVAILABILITY
  - Lead contact
  - Materials availability

SUPPLEMENTAL INFORMATION

Supplemental information can be found online at https://doi.org/10.1016/j.isci.2023.108703.

ACKNOWLEDGMENTS

This work was supported by grants from the National Key R&D Program of China (2019YFA0802600 and 2022YFC2703704) and the National Natural Science Foundation of China (81974244 and 81570960).

AUTHOR CONTRIBUTIONS

Conceptualization, L.L. and Y.S.; methodology, L.L., Y.S., and B.W.; data analysis, L.L., W.L., X.Y., Y.Z., and D.Y.; data curation, L.L. and M.S.; writing the article, L.L. and M.S.; supervision, M.S.; funding acquisition, M.S.

DECLARATION OF INTERESTS

The authors declare no competing interests.

INCLUSION AND DIVERSITY

We support inclusive, diverse, and equitable conduct of research.

Received: April 13, 2023
Revised: September 22, 2023
Accepted: December 6, 2023
Published: December 9, 2023

REFERENCES

1. Barker, D.J. (1990). The fetal and infant origins of adult disease. BMJ *301*, 1111.
2. Calkins, K., and Devaskar, S.U. (2011). Fetal origins of adult disease. Curr. Probl. Pediatr. Adolesc. Health Care *41*, 158–176.
3. Barker, D.J., Osmond, C., Golding, J., Kuh, D., and Wadsworth, M.E. (1989). Growth in utero, blood pressure in childhood and adult life, and mortality from cardiovascular disease. BMJ *298*, 564–567.
4. Barker, D.J.P., Osmond, C., Kajantie, E., and Eriksson, J.G. (2009). Growth and chronic disease: findings in the Helsinki Birth Cohort. Ann. Hum. Biol. *36*, 445–458.
5. Barker, D.J.P. (2005). The developmental origins of insulin resistance. Horm. Res. *64*, 2–7.
6. Lumey, L.H. (1992). Decreased birthweights in infants after maternal in utero exposure to the Dutch famine of 1944-1945. Paediatr. Perinat. Epidemiol. *6*, 240–253.
7. Roseboom, T., de Rooij, S., and Painter, R. (2006). The Dutch famine and its long-term consequences for adult health. Early Hum. Dev. *82*, 485–491.
8. Wiegersma, A.M., Boots, A., Roseboom, T.J., and de Rooij, S.R. (2022). Correction: Prenatal exposure to the Dutch famine is associated with more self-perceived cognitive problems at 72 years of age. BMC Geriatr. *22*, 413.
9. Boots, A., Thomason, M.E., Espinoza-Heredia, C., Pruitt, P.J., Damoiseaux, J.S., Roseboom, T.J., and de Rooij, S.R. (2022). Sex-specific effects of prenatal undernutrition on resting-state functional connectivity in the human brain at age 68. Neurobiol. Aging *112*, 129–138.

10. Giussani, D.A. (2021). Breath of Life: Heart Disease Link to Developmental Hypoxia. Circulation *144*, 1429–1443.
11. Leslie, E., Lopez, V., Anti, N.A.O., Alvarez, R., Kafeero, I., Welsh, D.G., Romero, M., Kaushal, S., Johnson, C.M., Bosviel, R., et al. (2021). Gestational long-term hypoxia induces metabolomic reprogramming and phenotypic transformations in fetal sheep pulmonary arteries. Am. J. Physiol. Lung Cell Mol. Physiol. *320*, L770–L784.
12. Walton, S.L., Singh, R.R., Little, M.H., Bowles, J., Li, J., and Moritz, K.M. (2018). Prolonged prenatal hypoxia selectively disrupts collecting duct patterning and postnatal function in male mouse offspring. J. Physiol. *596*, 5873–5889.
13. Wesolowski, S.R., Kasmi, K.C.E., Jonscher, K.R., and Friedman, J.E. (2017). Developmental origins of NAFLD: a womb with a clue. Nat. Rev. Gastroenterol. Hepatol. *14*, 81–96.
14. Wang, B., Zeng, H., Liu, J., and Sun, M. (2021). Effects of Prenatal Hypoxia on Nervous System Development and Related Diseases. Front. Neurosci. *15*, 755554.
15. Zhang, Y., Zhang, M., Li, L., Wei, B., He, A., Lu, L., Li, X., Zhang, L., Xu, Z., and Sun, M. (2018). Methylation-reprogrammed Wnt/beta-catenin signalling mediated prenatal hypoxia-induced brain injury in foetal and offspring rats. J. Cell Mol. Med. *22*, 3866–3874.
16. Wei, B., Li, L., He, A., Zhang, Y., Sun, M., and Xu, Z. (2016). Hippocampal NMDAR-Wnt-Catenin signaling disrupted with cognitive deficits in adolescent offspring exposed to prenatal hypoxia. Brain Res. *1631*, 157–164.
17. Zhuravin, I.A., Dubrovskaya, N.M., Vasilev, D.S., Kozlova, D.I., Kochkina, E.G., Tumanova, N.L., and Nalivaeva, N.N. (2019). Regulation of Neprilysin Activity and Cognitive Functions in Rats After Prenatal Hypoxia. Neurochem. Res. *44*, 1387–1398.
18. Vetrovoy, O., Stratilov, V., Nimiritsky, P., Makarevich, P., and Tyulkova, E. (2021). Prenatal Hypoxia Induces Premature Aging Accompanied by Impaired Function of the Glutamatergic System in Rat Hippocampus. Neurochem. Res. *46*, 550–563.
19. Tönnies, E., and Trushina, E. (2017). Oxidative Stress, Synaptic Dysfunction, and Alzheimer's Disease. J. Alzheimers Dis. *57*, 1105–1121.
20. Barthet, G., and Mulle, C. (2020). Presynaptic failure in Alzheimer's disease. Prog. Neurobiol. *194*, 101801.
21. Montero-Crespo, M., Domínguez-Álvaro, M., Alonso-Nanclares, L., DeFelipe, J., and Blazquez-Llorca, L. (2021). Three-dimensional analysis of synaptic organization in the hippocampal CA1 field in Alzheimer's disease. Brain *144*, 553–573.
22. Hirai, H., Pang, Z., Bao, D., Miyazaki, T., Li, L., Miura, E., Parris, J., Rong, Y., Watanabe, M., Yuzaki, M., and Morgan, J.I. (2005). Cbln1 is essential for synaptic integrity and plasticity in the cerebellum. Nat. Neurosci. *8*, 1534–1541.
23. Jin, Y., Zhang, B., Lu, J., Song, Y., Wang, W., Zhang, W., Shao, F., Gong, M., Wang, M., Liang, X., et al. (2021). Long noncoding RNA PM maintains cerebellar synaptic integrity and Cbln1 activation via Pax6/Mll1-mediated H3K4me3. PLoS Biol. *19*, e3001297.
24. Otsuka, S., Konno, K., Abe, M., Motohashi, J., Kohda, K., Sakimura, K., Watanabe, M., and Yuzaki, M. (2016). Roles of Cbln1 in Non-Motor Functions of Mice. J. Neurosci. *36*, 11801–11816.
25. Miura, E., Iijima, T., Yuzaki, M., and Watanabe, M. (2006). Distinct expression of Cbln family mRNAs in developing and adult mouse brains. Eur. J. Neurosci. *24*, 750–760.
26. Boo, S.H., and Kim, Y.K. (2020). The emerging role of RNA modifications in the regulation of mRNA stability. Exp. Mol. Med. *52*, 400–408.
27. Li, H., Ren, Y., Mao, K., Hua, F., Yang, Y., Wei, N., Yue, C., Li, D., and Zhang, H. (2018). FTO is involved in Alzheimer's disease by targeting TSC1-mTOR-Tau signaling. Biochem. Biophys. Res. Commun. *498*, 234–239.
28. Widagdo, J., and Anggono, V. (2018). The m6A-epitranscriptomic signature in neurobiology: from neurodevelopment to brain plasticity. J. Neurochem. *147*, 137–152.
29. Wang, C.X., Cui, G.S., Liu, X., Xu, K., Wang, M., Zhang, X.X., Jiang, L.Y., Li, A., Yang, Y., Lai, W.Y., et al. (2018). METTL3-mediated m6A modification is required for cerebellar development. PLoS Biol. *16*, e2004880.
30. Zaccara, S., Ries, R.J., and Jaffrey, S.R. (2019). Reading, writing and erasing mRNA methylation. Nat. Rev. Mol. Cell Biol. *20*, 608–624.
31. Wang, X., Lu, Z., Gomez, A., Hon, G.C., Yue, Y., Han, D., Fu, Y., Parisien, M., Dai, Q., Jia, G., et al. (2014). N6-methyladenosine-dependent regulation of messenger RNA stability. Nature *505*, 117–120.
32. Xiao, W., Adhikari, S., Dahal, U., Chen, Y.S., Hao, Y.J., Sun, B.F., Sun, H.Y., Li, A., Ping, X.L., Lai, W.Y., et al. (2016). Nuclear m(6)A Reader YTHDC1 Regulates mRNA Splicing. Mol. Cell *61*, 507–519.
33. Wang, X., Zhao, B.S., Roundtree, I.A., Lu, Z., Han, D., Ma, H., Weng, X., Chen, K., Shi, H., and He, C. (2015). N(6)-methyladenosine Modulates Messenger RNA Translation Efficiency. Cell *161*, 1388–1399.
34. Dominissini, D., Moshitch-Moshkovitz, S., Schwartz, S., Salmon-Divon, M., Ungar, L., Osenberg, S., Cesarkas, K., Jacob-Hirsch, J., Amariglio, N., Kupiec, M., et al. (2012). Topology of the human and mouse m6A RNA methylomes revealed by m6A-seq. Nature *485*, 201–206.
35. Zaccara, S., and Jaffrey, S.R. (2020). A Unified Model for the Function of YTHDF Proteins in Regulating m(6)A-Modified mRNA. Cell *181*, 1582–1595.e18.
36. Shi, H., Wang, X., Lu, Z., Zhao, B.S., Ma, H., Hsu, P.J., Liu, C., and He, C. (2017). YTHDF3 facilitates translation and decay of N(6)-methyladenosine-modified RNA. Cell Res. *27*, 315–328.
37. Tourrière, H., Chebli, K., and Tazi, J. (2002). mRNA degradation machines in eukaryotic cells. Biochimie *84*, 821–837.
38. Doidge, R., Mittal, S., Aslam, A., and Winkler, G.S. (2012). Deadenylation of cytoplasmic mRNA by the mammalian Ccr4-Not complex. Biochem. Soc. Trans. *40*, 896–901.
39. Chen, C.Y., and Shyu, A.B. (2011). Mechanisms of deadenylation-dependent decay. Wiley Interdiscip Rev RNA *2*, 167–183.
40. Liu, J., Lu, X., Zhang, S., Yuan, L., and Sun, Y. (2022). Molecular Insights into mRNA Polyadenylation and Deadenylation. Int. J. Mol. Sci. *23*, 10985.
41. Du, H., Zhao, Y., He, J., Zhang, Y., Xi, H., Liu, M., Ma, J., and Wu, L. (2016). YTHDF2 destabilizes m(6)A-containing RNA through direct recruitment of the CCR4-NOT deadenylase complex. Nat. Commun. *7*, 12626.
42. Mauxion, F., Faux, C., and Séraphin, B. (2008). The BTG2 protein is a general activator of mRNA deadenylation. EMBO J. *27*, 1039–1048.
43. Ramanan, V.K., Lesnick, T.G., Przybelski, S.A., Heckman, M.G., Knopman, D.S., Graff-Radford, J., Lowe, V.J., Machulda, M.M., Mielke, M.M., Jack, C.R., Jr., et al. (2021). Coping with brain amyloid: genetic heterogeneity and cognitive resilience to Alzheimer's pathophysiology. Acta Neuropathol. Commun. *9*, 48.
44. Kruszka, P., Berger, S.I., Weiss, K., Everson, J.L., Martinez, A.F., Hong, S., Anyane-Yeboa, K., Lipinski, R.J., and Muenke, M. (2019). A CCR4-NOT Transcription Complex, Subunit 1, CNOT1, Variant Associated with Holoprosencephaly. Am. J. Hum. Genet. *104*, 990–993.
45. Wang, J., Wang, K., Liu, W., Cai, Y., and Jin, H. (2021). m6A mRNA methylation regulates the development of gestational diabetes mellitus in Han Chinese women. Genomics *113*, 1048–1056.
46. Huong, T.T., Ngoc, L.N.T., and Kang, H. (2020). Functional Characterization of a Putative RNA Demethylase ALKBH6 in Arabidopsis Growth and Abiotic Stress Responses. Int. J. Mol. Sci. *21*, 6707.
47. Rouault, J.P., Prévôt, D., Berthet, C., Birot, A.M., Billaud, M., Magaud, J.P., and Corbo, L. (1998). Interaction of BTG1 and p53-regulated BTG2 gene products with mCaf1, the murine homolog of a component of the yeast CCR4 transcriptional regulatory complex. J. Biol. Chem. *273*, 22563–22569.
48. Camm, E.J., Cross, C.M., Kane, A.D., Tarry-Adkins, J.L., Ozanne, S.E., and Giussani, D.A. (2021). Maternal antioxidant treatment protects adult offspring against memory loss and hippocampal atrophy in a rodent model of developmental hypoxia. FASEB J *35*, e21477.
49. Scibelli, F., Fucà, E., Guerrera, S., Lupi, E., Alfieri, P., Valeri, G., and Vicari, S. (2021). Clinical and individual features associated with maternal stress in young adolescents with autism spectrum disorder. Autism Res. *14*, 1935–1947.
50. Giussani, D.A., Phillips, P.S., Anstee, S., and Barker, D.J. (2001). Effects of altitude versus economic status on birth weight and body shape at birth. Pediatr. Res. *49*, 490–494.
51. Soria, R., Julian, C.G., Vargas, E., Moore, L.G., and Giussani, D.A. (2013). Graduated effects of high-altitude hypoxia and highland ancestry on birth size. Pediatr. Res. *74*, 633–638.
52. Camm, E.J., Hansell, J.A., Kane, A.D., Herrera, E.A., Lewis, C., Wong, S., Morrell, N.W., and Giussani, D.A. (2010). Partial contributions of developmental hypoxia and undernutrition to prenatal alterations in somatic growth and cardiovascular structure and function. Am. J. Obstet. Gynecol. *203*, 495.e24–495.e34.
53. Brain, K.L., Allison, B.J., Niu, Y., Cross, C.M., Itani, N., Kane, A.D., Herrera, E.A., Skeffington, K.L., Botting, K.J., and Giussani, D.A. (2019). Intervention against hypertension in the next generation programmed by developmental hypoxia. PLoS Biol. *17*, e2006552.
54. Shen, G., Hu, S., Zhao, Z., Zhang, L., and Ma, Q. (2020). Antenatal Hypoxia Accelerates the Onset of Alzheimer's Disease Pathology in 5xFAD Mouse Model. Front. Aging Neurosci. *12*, 251.
55. Rumman, M., Pandey, S., Singh, B., Gupta, M., Ubaid, S., and Mahdi, A.A. (2021). Genistein Prevents Hypoxia-Induced

Cognitive Dysfunctions by Ameliorating Oxidative Stress and Inflammation in the Hippocampus. Neurotox. Res. *39*, 1123–1133.
56. Shaw, K., Bell, L., Boyd, K., Grijseels, D.M., Clarke, D., Bonnar, O., Crombag, H.S., and Hall, C.N. (2021). Neurovascular coupling and oxygenation are decreased in hippocampus compared to neocortex because of microvascular differences. Nat. Commun. *12*, 3190.
57. Terry, R.D., Masliah, E., Salmon, D.P., Butters, N., DeTeresa, R., Hill, R., Hansen, L.A., and Katzman, R. (1991). Physical basis of cognitive alterations in Alzheimer's disease: synapse loss is the major correlate of cognitive impairment. Ann. Neurol. *30*, 572–580.
58. Hong, S., Beja-Glasser, V.F., Nfonoyim, B.M., Frouin, A., Li, S., Ramakrishnan, S., Merry, K.M., Shi, Q., Rosenthal, A., Barres, B.A., et al. (2016). Complement and microglia mediate early synapse loss in Alzheimer mouse models. Science *352*, 712–716.
59. Hayashi, A., Nagaoka, M., Yamada, K., Ichitani, Y., Miake, Y., and Okado, N. (1998). Maternal stress induces synaptic loss and developmental disabilities of offspring. Int. J. Dev. Neurosci. *16*, 209–216.
60. Giannopoulou, I., Pagida, M.A., Briana, D.D., and Panayotacopoulou, M.T. (2018). Perinatal hypoxia as a risk factor for psychopathology later in life: the role of dopamine and neurotrophins. Hormones (Basel) *17*, 25–32.
61. Reemst, K., Noctor, S.C., Lucassen, P.J., and Hol, E.M. (2016). The Indispensable Roles of Microglia and Astrocytes during Brain Development. Front. Hum. Neurosci. *10*, 566.
62. Yuzaki, M. (2011). Cbln1 and its family proteins in synapse formation and maintenance. Curr. Opin. Neurobiol. *21*, 215–220.
63. Seigneur, E., and Südhof, T.C. (2018). Genetic Ablation of All Cerebellins Reveals Synapse Organizer Functions in Multiple Regions Throughout the Brain. J. Neurosci. *38*, 4774–4790.
64. Suzuki, K., Elegheert, J., Song, I., Sasakura, H., Senkov, O., Matsuda, K., Kakegawa, W., Clayton, A.J., Chang, V.T., Ferrer-Ferrer, M., et al. (2020). A synthetic synaptic organizer protein restores glutamatergic neuronal circuits. Science *369*, eabb4853.
65. Saffery, R., and Novakovic, B. (2014). Epigenetics as the mediator of fetal programming of adult onset disease: what is the evidence? Acta Obstet. Gynecol. Scand. *93*, 1090–1098.
66. Gluckman, P.D., Hanson, M.A., Cooper, C., and Thornburg, K.L. (2008). Effect of in utero and early-life conditions on adult health and disease. N. Engl. J. Med. *359*, 61–73.
67. Young, D.A. (1984). Advantages of separations on "giant" two-dimensional gels for detection of physiologically relevant changes in the expression of protein gene-products. Clin. Chem. *30*, 2104–2108.
68. Yue, Y., Liu, J., and He, C. (2015). RNA N6-methyladenosine methylation in post-transcriptional gene expression regulation. Genes Dev. *29*, 1343–1355.
69. Fu, Y., Dominissini, D., Rechavi, G., and He, C. (2014). Gene expression regulation mediated through reversible m(6)A RNA methylation. Nat. Rev. Genet. *15*, 293–306.
70. Meyer, K.D., Saletore, Y., Zumbo, P., Elemento, O., Mason, C.E., and Jaffrey, S.R. (2012). Comprehensive analysis of mRNA methylation reveals enrichment in 3' UTRs and near stop codons. Cell *149*, 1635–1646.
71. Chang, M., Lv, H., Zhang, W., Ma, C., He, X., Zhao, S., Zhang, Z.W., Zeng, Y.X., Song, S., Niu, Y., and Tong, W.M. (2017). Region-specific RNA m(6)A methylation represents a new layer of control in the gene regulatory network in the mouse brain. Open Biol. *7*, 170166.
72. Yoon, K.J., Ringeling, F.R., Vissers, C., Jacob, F., Pokrass, M., Jimenez-Cyrus, D., Su, Y., Kim, N.S., Zhu, Y., Zheng, L., et al. (2017). Temporal Control of Mammalian Cortical Neurogenesis by m(6)A Methylation. Cell *171*, 877–889.e17.
73. Wu, R., Li, A., Sun, B., Sun, J.G., Zhang, J., Zhang, T., Chen, Y., Xiao, Y., Gao, Y., Zhang, Q., et al. (2019). A novel m(6)A reader Prrc2a controls oligodendroglial specification and myelination. Cell Res. *29*, 23–41.
74. Yu, J., Chen, M., Huang, H., Zhu, J., Song, H., Zhu, J., Park, J., and Ji, S.J. (2018). Dynamic m6A modification regulates local translation of mRNA in axons. Nucleic Acids Res. *46*, 1412–1423.
75. Livneh, I., Moshitch-Moshkovitz, S., Amariglio, N., Rechavi, G., and Dominissini, D. (2020). The m(6)A epitranscriptome: transcriptome plasticity in brain development and function. Nat. Rev. Neurosci. *21*, 36–51.
76. Pan, T., Wu, F., Li, L., Wu, S., Zhou, F., Zhang, P., Sun, C., and Xia, L. (2021). The role m(6)A RNA methylation is CNS development and glioma pathogenesis. Mol. Brain *14*, 119.
77. Liu, X., Shimada, T., Otowa, T., Wu, Y.Y., Kawamura, Y., Tochigi, M., Iwata, Y., Umekage, T., Toyota, T., Maekawa, M., et al. (2016). Genome-wide Association Study of Autism Spectrum Disorder in the East Asian Populations. Autism Res. *9*, 340–349.
78. Milaneschi, Y., Lamers, F., Mbarek, H., Hottenga, J.J., Boomsma, D.I., and Penninx, B.W.J.H. (2014). The effect of FTO rs9939609 on major depression differs across MDD subtypes. Mol. Psychiatry *19*, 960–962.
79. Han, M., Liu, Z., Xu, Y., Liu, X., Wang, D., Li, F., Wang, Y., and Bi, J. (2020). Abnormality of m6A mRNA Methylation Is Involved in Alzheimer's Disease. Front. Neurosci. *14*, 98.
80. Reitz, C., Tosto, G., Mayeux, R., and Luchsinger, J.A.; NIA-LOAD/NCRAD Family Study Group; Alzheimer's Disease Neuroimaging Initiative (2012). Genetic variants in the Fat and Obesity Associated (FTO) gene and risk of Alzheimer's disease. PLoS One *7*, e50354.
81. Li, M., Zhao, X., Wang, W., Shi, H., Pan, Q., Lu, Z., Perez, S.P., Suganthan, R., He, C., Bjørås, M., and Klungland, A. (2018). Ythdf2-mediated m(6)A mRNA clearance modulates neural development in mice. Genome Biol. *19*, 69.
82. Zhang, C., Samanta, D., Lu, H., Bullen, J.W., Zhang, H., Chen, I., He, X., and Semenza, G.L. (2016). Hypoxia induces the breast cancer stem cell phenotype by HIF-dependent and ALKBH5-mediated m(6)A-demethylation of NANOG mRNA. Proc. Natl. Acad. Sci. USA *113*, E2047–E2056.
83. Song, H., Feng, X., Zhang, H., Luo, Y., Huang, J., Lin, M., Jin, J., Ding, X., Wu, S., Huang, H., et al. (2019). METTL3 and ALKBH5 oppositely regulate m(6)A modification of TFEB mRNA, which dictates the fate of hypoxia/reoxygenation-treated cardiomyocytes. Autophagy *15*, 1419–1437.
84. Liu, J., Gao, M., Xu, S., Chen, Y., Wu, K., Liu, H., Wang, J., Yang, X., Wang, J., Liu, W., et al. (2020). YTHDF2/3 Are Required for Somatic Reprogramming through Different RNA Deadenylation Pathways. Cell Rep. *32*, 108120.
85. Du, H., Zou, N.Y., Zuo, H.L., Zhang, X.Y., and Zhu, S.C. (2023). YTHDF3 mediates HNF1alpha regulation of cervical cancer radio-resistance by promoting RAD51D translation in an m6A-dependent manner. FEBS J. *290*, 1920–1935.
86. Rueda-Clausen, C.F., Stanley, J.L., Thambiraj, D.F., Poudel, R., Davidge, S.T., and Baker, P.N. (2014). Effect of prenatal hypoxia in transgenic mouse models of preeclampsia and fetal growth restriction. Reprod. Sci. *21*, 492–502.
87. Zeng, H., Wei, B., Liu, J., Lu, L., Li, L., Wang, B., and Sun, M. (2022). Hypoxia-inducible Factor Regulates Ten-eleven Translocated Methylcytosine Dioxygenase 1-c-Myc Binding Involved in Depression-like Behavior in Prenatal Hypoxia Offspring. Neuroscience *502*, 41–51.
88. Spencer, J.L., Waters, E.M., Romeo, R.D., Wood, G.E., Milner, T.A., and McEwen, B.S. (2008). Uncovering the mechanisms of estrogen effects on hippocampal function. Front. Neuroendocrinol. *29*, 219–237.
89. Lovick, T.A. (2012). Estrous cycle and stress: influence of progesterone on the female brain. Braz. J. Med. Biol. Res. *45*, 314–320.
90. Morris, R. (1984). Developments of a water-maze procedure for studying spatial learning in the rat. J. Neurosci. Methods *11*, 47–60.
91. Liu, Y., Zhang, Y., Zheng, X., Fang, T., Yang, X., Luo, X., Guo, A., Newell, K.A., Huang, X.F., and Yu, Y. (2018). Galantamine improves cognition, hippocampal inflammation, and synaptic plasticity impairments induced by lipopolysaccharide in mice. J. Neuroinflammation *15*, 112.
92. Lourenco, M.V., Frozza, R.L., de Freitas, G.B., Zhang, H., Kincheski, G.C., Ribeiro, F.C., Gonçalves, R.A., Clarke, J.R., Beckman, D., Staniszewski, A., et al. (2019). Exercise-linked FNDC5/irisin rescues synaptic plasticity and memory defects in Alzheimer's models. Nat. Med. *25*, 165–175.

STAR★METHODS

KEY RESOURCES TABLE

REAGENT or RESOURCE	SOURCE	IDENTIFIER
Antibodies		
Anti-CBLN1	Abcam	Cat# ab181379
Synaptophysin polyclonal antibody	Proteintech	Cat# 17785-1-AP; RRID: AB_2271365
YTHDF3-specific polyclonal antibody	Proteintech	Cat# 25537-1-AP; RRID: AB_2847817
PSD95-specific polyclonal antibody	Proteintech	Cat# 20665-1-AP; RRID: AB_2687961
beta Tubulin III Rabbit Recombinant mAb	Bimake	Cat# A5107
Beta Actin Monoclonal antibody	Proteintech	Cat# 66009-1-Ig; RRID: AB_2687938
Anti- YTHDF3	SANTA CRUZ	Cat# sc-377119; RRID: AB_2687436
m^6A antibody	Proteintech	Cat# 68055-1-Ig; RRID: AB_2918796
Normal mouse IgG	SANTA CRUZ	Cat# sc-2025; RRID: AB_737182
Biological samples		
Hippocampus tissues	C57BL/6J	www.vitalriver.com
Chemicals, peptides, and recombinant proteins		
Pentobarbital sodium salt	Sigma	Cat.No:P3761
actinomycin D	Sigma	Cat.No:A1410
Methylene blue	MCE	Cat.No:HY-14536
Dynabeads™ Protein G	Thermo Fisher Scientific	Cat.No:10003D
TRIzol Reagent	Thermo Fisher Scientific	Cat.No:15596026
RNase inhibitors	Thermo Fisher Scientific	Cat.No:10777019
MEM medium	Procell Life Science & Technology Company	Cat.No:PM150410
Fetal Bovine Serum	Procell Life Science & Technology Company	Cat.No:164210
Penicillin-Streptomycin Solution	Procell Life Science & Technology Company	Cat.No:PB180120
Critical commercial assays		
TB Green *Premix Ex Taq*™	Takara	Cat.No:RR420A
RevertAid First Strand cDNA Synthesis Kit	Thermo Scientific	Cat.No:K1622
RIPA buffer	Beyotime	Cat.No:P0013K
Detergent Compatible Bradford Protein Assay Kit	Beyotime	Cat.No:P0006C-2
IP lysis buffer	Beyotime	Cat.No:P0013
Lipofectamine 2000	Invitrogen	Cat.No:11668019
FD Rapid Golgistain Kit	FD Neurotechnologies Inc.	Cat.No:PK401C
Dual-Luciferase Reporter Assay Kit	Vazyme	Cat.No:DL101-01
Nissl staining kit	Solarbio	Cat.No:G1436
TruSeq PE Cluster Kit v3-cBot-HS	Illumia	Cat.No:PE-401-3001
Deposited data		
Raw and analyzed data	This paper	GEO:GSE249147
Experimental models: Cell lines		
Neuro-2a (N2a) cell line	Procell Life Science & Technology Company	Cat.No:CL-0168
Experimental models: Organisms/strains		
C57BL/6J	This paper	www.vitalriver.com

(*Continued on next page*)

Continued

REAGENT or RESOURCE	SOURCE	IDENTIFIER
Oligonucleotides		
siRNA targeting sequence: *Ythdf3* sense: GCAGUGGUAUGACUAGCAUTT Antisense: AUGCUAGUCAUACCACUGCTT	This paper	N/A
siRNA targeting sequence: *Cbln1* sense: GGUGAAAGUCUACAACAGATT Antisense: UCUGUUGUAGACUUUCACCTT	This paper	N/A
siRNA targeting sequence: *Btg2* sense: GGACGCACUGACCGAUCAUTT Antisense: AUGAUCGGUCAGUGCGUCCTT	This paper	N/A
siRNA targeting sequence: Negativecontrol (NC): sense:UUCUCCGAACGUGUCACGUTT Antisense:ACGUGACACGUUCGGAGAATT	This paper	N/A
Recombinant DNA		
pcDNA3.1-*Ythdf3*	Sangon Biotech	N/A
pcDNA3.1 vector	Sangon Biotech	N/A
pmirGLO-*Cbln* 3′UTR Wild type	GenePharma Company	N/A
pmirGLO- *Cbln* 3′UTR Mutant	GenePharma Company	N/A
Software and algorithms		
Bio-Rad CFX96 PCR System	Bio-Rad	N/A
UVP Bio-imaging system EC3 apparatus	GE Healthcare	N/A
ANY-maze system	Stoelting Company	N/A
Rotarod apparatus	Anhui Zhenghua Biologic Apparatus Facilities	Cat.No:ZH-600B
ImageJ software	National Institutes of Health	https://ImageJ.nih.gov/ij/
GraphPad (Prism 8.4.2)	GraphPad	http://www.graphpad.com
Other		
NC membrane	Pall Corporation	Cat.No:66485
UV light	www.yunhoe.com	Cat.No:UVPL-4
Nitrocellulose filter membrane	Merck Millipore	Cat.No:HATF00010

RESOURCE AVAILABILITY

Lead contact

Further information and requests for resources and reagents should be directed to and will be fulfilled by the lead contact, Miao Sun (miaosunsuda@163.com)

Materials availability

This study did not generate new unique reagents.

Data and code availability

Data: Raw and analyzed sequencing data have been deposited at Gene Expression Omnibus (GEO, accession number: GSE249147) and are publicly available as of the date publication. Accession number is listed in the key resources table.

Code: This paper does not report original code.

Other items: Any additional information required to reanalyze the data reported in this paper is available from the lead contact upon request.

EXPERIMENTAL MODEL AND STUDY PARTICIPANT DETAILS

Animals

All procedures relating to animal care and treatment were performed according to the guidelines set by the Animal Resource Committee of Soochow University. Mice were sacrificed after anesthesia with sodium pentobarbital (30 mg/kg, ip).

The C57BL/6J mice were obtained from the Experimental Animal Center of Soochow University. Pregnancy was confirmed by detecting vaginal mucus plugs, and the morning of sighting a vaginal plug was denoted as day 0.5 of pregnancy [gestational day (GD) 0.5]. Pregnant mice were randomly divided into the control (Ctrl) group and prenatal hypoxia (PH) groups. The PH model was induced in pregnant mice by exposing them to a low oxygen environment of 10.5% from GD 12.5 to GD 17.5, whereas the control group was kept in a normal oxygen chamber with 21.0% oxygen concentration.[86,87] Once the modeling period was complete, the pregnant mice were transferred back to a normal environment and allowed to give birth naturally. After weaning, male and female offspring were housed in separate cages. All the mice were housed five per cage on a 12:12 h light/dark cycle at 22 ± 1°C with free access to food and water.

All behavioral tests were conducted on 2-month-old offspring by an investigator blinded to the progeny group during the light cycle. It should be pointed out that since several studies have shown that estrogen, estrous cycle, etc. will have a certain impact on the cognitive function of female mice,[88,89] in order to exclude the interference of such confounding factors, all subsequent experiments in this study were conducted on male offspring.

Mammalian cell culture

Neuro-2a (N2a) cell line used in this study was purchased from Procell Life Science & Technology Company (CAS Number: CL-0168) and grown in medium for N2a cells (CAS Number: CM-0168) consist of MEM (PM150410) + 10% FBS (164210-500) + 1% P/S (PB180120) at 37°C and 5% CO_2.

As for the hypoxia model *in vitro*, N2a cells were treated with 3% O_2 and 5% CO_2 at 37°C when N2a cells reached 80% of confluence. After 12 h hypoxia, total RNA and protein were isolated for Quantitative Real-Time Polymerase Chain Reaction (RT-qPCR) and immunoblot analysis.

METHOD DETAILS

Morris water maze (MWM)

The MWM was utilized to determine the spatial learning and memory of the offspring in two groups as described previously.[90] In brief, the mice were trained to find the underwater platform (26 cm in height and 10 cm in diameter) in a circular pool (46 cm in depth and 120 cm in diameter). The duration of the experiment was five days, including the positioning navigation trial (PNT, from day 1 to day 4) and the space probe trial (SPT, day 5). During the PNT period, mice were placed in one of four pool quadrants facing the tank wall, and then a computer tracking program was started when the animal was released. The video camera system will stop recording when the animal reaches the platform. A trial limit of 1 min is standard, and animals not finding the platform within this time limit were placed on the platform. Each animal was given four trials per day. On subsequent days, the trials were repeated. With four trials per day, four days (16 trials) is typically sufficient in a 120 cm water maze for the mouse to reach asymptotic performance. Latency to platform, travel distance, and swim speed were recorded. On day 5, the platform was removed from the pool, and then the animals were placed in a novel start position in the maze (180° from the original platform position) facing the tank wall. The purpose of the SPT is to evaluate whether or not the animal recalls the location of the platform. The time of this trial is 1 min, and the number of platform-site crossovers and time spent in the target quadrant (the quadrant where the platform is located) were recorded. All activities of mice in tests were recorded and analyzed using the ANY-maze system (Stoelting Company, Tokyo, Japan).

Step-through tests

The step-through test was conducted to evaluate memory acquisition as stated earlier.[91] Briefly, the test included a training trial on the first day and a retention trial on the second day. The apparatus consisted of a compartment with two chambers (a light chamber equipped with an illuminator and a dark chamber) and an interconnecting semicircular door. During the training trial, the mice were placed in the light chamber for 3 min. After the door opened, the mice moved to the dark chamber and received a footshock for 1 s, 0.4 mA. During the 5 min retention trial, the number of mistakes (entering the dark chamber) and the time that the mice took before initially entering the dark chamber (the step-through latency) were recorded.

Novel object recognition (NOR)

Object recognition tests were carried out in an open field arena measuring 0.3 m long × 0.3 m wide × 0.45 m high, as previously described.[92] In brief, animals were trained in a 5 min-long session during which they were placed at the center of the arena in the presence of two identical objects. Exploratory behavior (amount of time spent exploring each object) was recorded using the ANY-maze system. 4 h after training, animals were replaced in the arena for the test session, in which one of the objects had been replaced by a different (novel) object. Again, time spent exploring familiar and novel objects was measured. Animals with a total exploration time below 10 s were excluded from NOR tests. Results are expressed as a percentage of time spent exploring a novel object during the test session and were analyzed using a one-sample Student's *t* test.

Rotarod test

The rotarod apparatus (Zhenghua, Anhui, China) was used to assess motor coordination. All mice were pre-trained on the rotarod apparatus to reach a stable performance. The training consisted of two consecutive days. Each day included three separate test trials, and each trial required the animal to stay on the rotarod for 300 s at 5 rpm. The final test (three trials, each trial lasting 300 s) was performed on the third day with the rod accelerated from 0 to 40 rpm. Between trials, mice were given at least 30 min of rest to reduce stress and fatigue. The average time stayed on the rod for three trials (latency), and the drop speed was recorded.

Nissl staining

The whole-brain tissue (4 mice in each group) was placed in 4% paraformaldehyde for fixation. The fixed brain tissue was dehydrated and transparent through the gradient of alcohol and xylene. Afterward, the brain was embedded in paraffin and sectioned by a microtome. Finally, the brain slices were stained using a Nissl staining kit (Solarbio, Beijing, China).

Quantitative real-time PCR (RT-qPCR)

Total RNA was extracted from hippocampal tissue or N2a cells using a TRIZOL reagent (15596026, Thermo Fisher Scientific). Then the purified total RNA (about 1 μg) was reverse-transcribed using the RevertAid First Strand cDNA Synthesis Kit (K1622, Thermo Scientific) according to the manufacturer's instructions. The messenger RNA (mRNA) expression was determined by RT-qPCR using a Bio-Rad CFX96 PCR System. All measurements were performed in triplicate, and the relative levels of mRNA were normalized for each sample with the expression levels of the reference gene using the $2^{-\Delta\Delta CT}$ method. Information regarding the sequences of gene-specific primers is provided in Table S1.

Immunoblot analysis

Hippocampal tissues or N2a cell lines were lysed in RIPA buffer (P0013K, Beyotime) with protease inhibitors (P002, NCM Biotech), then put on ice cracked for 30 min. After centrifugation at 13,800 g for 30 min at 4°C, the supernatant was extracted, and the protein concentration was measured according to the instructions of the Detergent Compatible Bradford Protein Assay Kit (P0006C-2, Beyotime). The remaining supernatant was denatured at 96°C for 15 min and subjected to immunoblot analysis. Protein (20 μg) was loaded to SDS-PAGE gels and transferred to the NC membrane (66485, Pall Corporation). The membranes were incubated with the antibodies against YTHDF3 (25537-1-AP, Proteintech), CBLN1 (ab181379, Abcam), SYN (17785-1-AP, Proteintech), PSD95 (20665-4-AP, Proteintech), TUBULIN (A5107, Bimake), and β-ACTIN (66009-1-Ig, Proteintech) overnight at 4°C. After washing with PBS/Tween Buffer (PS102, Epizyme Biotech), the membranes were incubated with secondary antibodies (goat anti-mouse for and β-ACTIN, goat anti-rabbit for YTHDF3, CBLN1, SYN, PSD95, and TUBULIN) for 1 h at room temperature. The protein bands were visualized using enhanced chemiluminescence (ECL) detection system (GE Healthcare, Piscataway, NJ, USA). Results were quantified using a UVP Bio-imaging system EC3 apparatus (UVP, Upland, CA, USA).

siRNA knockdown and plasmid transfection

Cells were seeded in 6-well plates. After 24 h, 75 nM siRNA was transfected using GP-transfect-Mate transfection reagent (GenePharma, China) according to the manufacturer's instructions. Cells were harvested two days following the initial transfection. Knockdown was validated prior to all experiments reported in this study by immunoblot analysis. Negative control siRNA from GenePharma was used as control siRNA in knockdown experiments. *Ythdf3* siRNA, *Cbln1* siRNA, and *Btg2* siRNA were also ordered from GenePharma. Table S2 shows the siRNA sequences used in gene knockdown experiments. In addition, *Ythdf3* CDS was synthesized by Sangon Biotech Company (Sangon Biotech Co., Ltd., Shanghai, China) and inserted into pcDNA3.1(+) Vector using the HindIII or XhoI restriction sites. 1.5 μg plasmid were transfected into N2a cells using lipofectamine 2000 (Invitrogen) in overexpression experiments. Overexpression was also validated prior to all experiments reported in this study by immunoblot analysis.

mRNA stability assay

N2a cell lines were transfected with *Ythdf3* siRNA. 48 h after the first transfection, actinomycin D (AcD) (5 μg/mL, A1410, Sigma) was added into the cell culture medium for the indicated times, and the mRNA levels of *Cbln1* at each time point (0 h, 2 h, and 4 h after the treatment with AcD) were analyzed by RT-qPCR.

UV-RIP-qPCR

UV-RIP-qPCR was performed as described previously.[23] In brief, for the UV-RIP-qPCR, homogenized hippocampal tissues were irradiated with UV light (400 mJ/cm^2, UVPL-4, Suzhou Yunhoe Electronic Technology Co., Ltd.). After centrifuging at 13,800 g at 4°C for 10 min, the hippocampal tissues were lysed for 30 min in RIPA buffer (P0013K, Beyotime) supplemented with RNase inhibitors (10777019, Thermo Fisher Scientific) and protease inhibitor cocktail (P002, NCM Biotech). After centrifuging at 13,800 g for 10 min at 4°C, the supernatant was precleared with 25 μL of Dynabeads Protein G (10003D, Thermo Fisher Scientific) at 4°C for 2 h. Then, the precleared lysate was incubated with 50 μL of Dynabeads Protein G that was precoated with 4 μg of normal mouse IgG (sc-2025, SANTA CRUZ) or YTHDF3 antibody (sc-377119, SANTA CRUZ) overnight. Then the beads were washed five times using RIPA buffer. Finally, RNA was extracted using TRIzol Reagent (15596026, Thermo Fisher Scientific). The protein-bound RNA was analyzed by RT-qPCR.

RNA sequencing (RNA-seq)

RNA sequencing was performed by the company (Beijing Nuohe Zhiyuan Technology Co., Ltd). In brief, a total amount of 3 μg RNA per sample was used as input material for the RNA sample preparations. Sequencing libraries were generated using NEBNext UltraTM RNA Library Prep Kit for Illumina (NEB, USA) following manufacturer's recommendations and index codes were added to attribute sequences to each sample. The clustering of the index-coded samples was performed on a cBot Cluster Generation System using TruSeq PE Cluster Kit v3-cBot-HS (Illumia) according to the manufacturer's instructions. After cluster generation, the library preparations were sequenced on an Illumina Hiseq platform and 125 bp/150 bp paired-end reads were generated. Follow-up data quality control and analysis were also carried out by the company (Beijing Nuohe Zhiyuan Technology Co., Ltd). Differentially expressed genes in RNA-seq results is provided in Table S3.

m^{6}A dot blot

Total RNAs were extracted, and the concentrations were adjusted by serial dilution to 100 ng/μL and 250 ng/μL for one assay. Total RNAs were denatured at 95°C for 3 min to disrupt any secondary structures. Then, 2 μL of serially diluted RNAs was dropped onto a nitrocellulose filter membrane (Merck Millipore, HATF00010) and crosslinked by ultraviolet for 1 h. After this, the membrane was washed and blocked in blocking buffer (5% milk in phosphate-buffered saline with 0.1% Tween 20) for 1 h at room temperature and subsequently incubated overnight at 4°C with anti-m^{6}A antibody (Proteintech, 68055-1-Ig). After washing twice, HRP-linked secondary antibody was diluted 1:5000 and incubated with the membranes for 1 h at room temperature and exposed to ECL substrate. The same amount of total RNAs were spotted on the membrane, stained with 0.02% methylene blue in 0.3M sodium acetate (pH 5.2) for 2 h at room temperature and washed with ribonuclease-free water for 5 h.

Golgi staining

The brains of mice at 2 months old were dissected and washed in Milli-Q water to remove blood from the surface. The brains were immersed in a 1:1 mixture of FD solution A:B (FD Neurotechnologies Inc., FD Rapid Golgistain Kit, PK401C) at room temperature for 14 days, followed by incubation in FD solution C at room temperature and in the dark for 7 days. The brains were then sectioned on a cryostat and mounted on gelatin-coated slides with FD solution C, dried naturally at room temperature. Staining procedures were followed per the manufacturer's instructions. Spine density was measured on pyramidal neurons that were located in the CA1 region of the dorsal hippocampus.

Methylated RNA immunoprecipitation sequencing (MeRIP-seq)

The RNA m^{6}A was sequenced by MeRIP-seq at Novogene (Beijing, China). Briefly, a total of 2 μg RNAs were extracted from the hippocampal tissue of two groups. The integrity and concentration of extracted RNAs were detected using Agilent 2100 bioanalyzer (Agilent) and simpliNano spectrophotometer (GE Healthcare), respectively. Fragmented RNA (~100 nt) was incubated for 2 h at 4°C with an anti-m^{6}A polyclonal antibody (Merk Millipore) in the immunoprecipitation experiment. Then, immunoprecipitated RNAs or input were used for library construction with Ovation SoLo RNA-Seq System Core Kit (NuGEN). The library preparations were sequenced on an Illumina Novaseq or Hiseq platform with a paired-end read length of 150 bp according to the standard protocols. Follow-up data quality control and analysis were carried out by the company (Beijing Nuohe Zhiyuan Technology Co., Ltd). Importantly, genome used for aligning the transcripts in the MeRIP-seq was "GRCm39/mm39".

Dual-luciferase reporter assay

DNA fragment corresponding to *Cbln1* 3′UTR in this assay was synthesized by GenePharma Company and inserted into pmirGLO vector using the SacI or XhoI restriction sites. The *Cbln1*-3′UTR mutant was also directly synthesized by replacing the A (adenosine) with C (cytosine) in the m^{6}A motif. All plasmids and mutations were verified by sequencing. 0.15 μg reporter plasmid was transfected into N2a cells in a 24-well plate using lipofectamine 2000 (Invitrogen) after knockdown or overexpression of *Ythdf3*. After 24 h, cell extracts were obtained, and Firefly/Renilla luciferase activities were measured using a Dual-Luciferase Reporter Assay Kit (DL101-01, Vazyme, China).

QUANTIFICATION AND STATISTICAL ANALYSIS

All data were expressed as the mean ± SEM and analyzed by GraphPad (Prism 8.4.2) software. Statistical analyses were performed via one-way/two-way analysis of variance (ANOVA) followed by the Bonferroni test or a two-tailed unpaired Student's *t* test. p values <0.05 were considered statistically significant. In each graph, otherwise specifically mentioned, ns, no significance; *, $p < 0.05$; **, $p < 0.01$; ***, $p < 0.001$ vs. control.